

Parameterizing individual effects of shear and stratification on mixing in stably stratified shear flows

Kenji Shimizu^{1,2,3}

Received 15 August 2011; revised 17 November 2011; accepted 27 January 2012; published 20 March 2012.

[1] This study proposes new parameterizations of diapycnal mixing by reanalyzing the results of previous laboratory and numerical experiments on homogeneous stably stratified shear flows. Unlike previous studies that use either the turbulent Froude number Fr or gradient Richardson number Ri_g , this study parameterizes nondimensional momentum and buoyancy fluxes as functions of Fr and a turbulent shear number Sh , in order to quantify individual effects of shear and stratification. Turbulent momentum flux is found to depend linearly on Sh and to decrease monotonically with decreasing Fr . Turbulent buoyancy flux has a peak at moderate Fr . With increasing Sh , it decreases and increases at high and low Fr , respectively. The increase of Sh also cause relatively small but significant decreases of nondimensional turbulent properties, such as the nondimensional conversion rate of turbulent potential energy to background potential energy. The proposed parameterizations lie within the scatter of limited available field data. The parameterizations may be reduced to Ri_g -based ones by incorporating the relationship between Ri_g and turbulence intensity observed in the field. Existing stability functions for two-equation turbulent closure schemes are found to over-predict mixing efficiency at low Fr .

Citation: Shimizu, K. (2012), Parameterizing individual effects of shear and stratification on mixing in stably stratified shear flows, *J. Geophys. Res.*, 117, C03030, doi:10.1029/2011JC007514.

1. Introduction

[2] Parameterizing diapycnal mixing in stratified shear flows is an essential component in a variety of problems in oceanography, geophysical fluid dynamics, and associated engineering. Some examples include thermohaline circulation; momentum, heat, and mass transfer across boundary layers; and fate and transport of sediment particles, nutrients, and pollutants.

[3] The effects of stratification on turbulence are often analyzed using the turbulent Froude number Fr or the gradient Richardson number Ri_g in laboratory studies [e.g., Rohr *et al.*, 1984, 1988b; Yoon and Warhaft, 1990], Direct Numerical Simulation (DNS) or Large Eddy Simulation (LES) studies [e.g., Holt *et al.*, 1992; Kaltenbach *et al.*, 1994; Shih *et al.*, 2000, 2005], and field studies [e.g., Peters *et al.*, 1995; Stacey *et al.*, 1999; Yeates, 2008]. These nondimensional numbers are defined as

$$Fr = \frac{q}{Nl}, \quad Ri_g = \frac{N^2}{S^2}, \quad (1)$$

where l is some characteristic length scale of turbulence (discussed later), q is the magnitude of turbulent velocity

fluctuation, N is the buoyancy frequency, and S is the shear. Fr and Ri_g are a common choice for unsheared and sheared stratified flows, respectively, and Fr has also been found useful for sheared flows [Kaltenbach *et al.*, 1994; Shih *et al.*, 2000]. However, parameterizations in terms of either Fr or Ri_g miss some important effects in stratified and sheared turbulence: Fr may be seen as a ratio of turbulence time scale relative to the buoyancy frequency and is independent of shear, whereas Ri_g measures relative effects of background shear and stratification and is independent of turbulence.

[4] One way to develop more comprehensive mixing parameterizations is to use more than one nondimensional variable, including a measure of shear relative to turbulence. Such a nondimensional variable is

$$Sh = \frac{Sl}{q}, \quad (2)$$

which is often defined with the length scale

$$l_d = \frac{q^3}{\varepsilon}. \quad (3)$$

This nondimensional variable is referred as the shear number in this study (the notation Sh is from Kaltenbach *et al.* [1994]). It is one of the important nondimensional parameters in unstratified shear flows, and it takes a relatively narrow range of values around 10 in the fully developed stage of homogeneous shear flows at high Reynolds numbers [e.g., Rogallo, 1981; Tavoularis and Karnik, 1989;

¹RPS MetOcean Pty Ltd., Jolimont, Western Australia, Australia.

²Also at Kitami Institute of Technology, Hokkaido, Japan.

³Now at Max-Planck-Institut für Meteorologie, Hamburg, Germany.

Lee *et al.*, 1990]. (Note that the terminal value tends to be ≈ 9 in unstratified shear flows [Rohr *et al.*, 1988a; Tavoularis and Karnik, 1989], but ≈ 11 in stratified shear flows [Rohr *et al.*, 1988b; Shih *et al.*, 2000, 2005].) However, Sh is included in the analysis of stratified shear flows relatively recently [Jacobitz *et al.*, 1997; Piccirillo and van Atta, 1997; Shih *et al.*, 2000, 2005], and as far as I am aware, there is no mixing parameterization in terms of both Sh and Fr (or Ri_g) based on experimental results. Stability functions for two-equation closure schemes [e.g., Kantha and Clayson, 1994; Canuto *et al.*, 2001] are examples of such parameterizations, but they are inconsistent with experimental data under strong stratification, as shown later in this study.

[5] To develop a mixing parameterization that includes the effects of both shear and stratification, it is natural to use Sh and Fr , considering stratified shear flows as a general case of unstratified shear flows and unsheared stratified flows. The shear effects represented by Sh are not captured well by a parameterization based only on Ri_g . To see this, note that Sh , Fr , and Ri_g are connected by the relationship [Kaltenbach *et al.*, 1994]

$$Ri_g = Sh^{-2}Fr^{-2}, \quad (4)$$

provided that the same length scale is used for Sh and Fr . The results of this study suggest that if (3) is used to define Sh and Fr , Sh typically varies by a factor of $2 \sim 3$ and Fr by orders of magnitude. This means that the variation of Fr or Ri_g is dominant, and relatively small but significant effects due to the variation of Sh need to be considered separately.

[6] The choice of length scale l is a critical factor that changes the outcome of mixing parameterizations based on these nondimensional numbers. In studies of stratified flows, it is common to use Ellison scale l_E [Ellison, 1957] or Thorpe displacement scale l_T [Thorpe, 1977], whereas studies of unstratified shear flows use l_d to define Sh . (Hereafter, the subscripts E , T , and d are used to denote variables defined with l_E , l_T , and l_d , respectively.) This study uses l_d for both Sh and Fr to take advantage of the relatively small variation in Sh_d and relationship (4), which allow us to convert the resulting parameterizations to Ri_g -based ones. Although there is a close relationship between Fr_d and Ri_g as mentioned above, the use of Fr_d is more advantageous because both unsheared and sheared cases may be combined to develop one parameterization common to both cases. The use of l_d has another advantage that in unstratified cases, $Fr_d \rightarrow \infty$ whereas Fr_E and Fr_T are undefined. In order to avoid dealing with infinity in unstratified cases, Fr_d^{-1} is used instead of Fr_d in the rest of this paper, following Kaltenbach *et al.* [1994].

[7] One approach to parameterize mixing is to analyze the results of laboratory experiments, DNS, and LES on stratified shear flows. An advantage of this approach is the availability of averaged turbulent quantities under controlled mean flow conditions, unlike microstructure measurements in the field that capture only a ‘snapshot’ of evolving turbulence, that results in large scatter due to its patchiness and intermittency. Such parameterizations may not be applicable to field conditions because of, for example, large Reynolds number difference, inhomogeneity, and the presence of stochastic internal waves [e.g., Gregg, 1989; Kunze *et al.*,

1990; Polzin *et al.*, 1995; Polzin, 1996]. There are also many sources of Turbulent Kinetic Energy (TKE) other than mean shear in the field, such as wind stirring in a surface mixed layer, surface wave breaking [Drennan *et al.*, 1996; Terray *et al.*, 1996], topographically induced internal waves [Toole *et al.*, 1994; Polzin *et al.*, 1997; Ledwell *et al.*, 2000; Moum *et al.*, 2002], and shear-induced static instability in bottom boundary layers [Moum *et al.*, 2004; Lorke *et al.*, 2005]. Nonetheless, shear is one of the important sources of TKE, and some turbulent quantities, such as length scale ratios and so-called mixing efficiencies, are comparable in laboratory or numerical experiments and in the field [e.g., Smyth *et al.*, 2001]. It is also easier to investigate a new aspect in an idealized condition, and the results would provide insight toward a better understanding of more general cases, such as field conditions.

[8] The purpose of this study is to develop parameterizations of mixing that include individual effects of shear and stratification, represented by Sh_d and Fr_d^{-1} . This is done by reanalyzing the results of previous laboratory and numerical experiments on (nearly) homogeneous stratified and sheared turbulence because many data sets are available and it is the simplest case in stratified shear flows. Since turbulence is driven by mean shear in these experiments, this choice excludes mixing driven by stochastic internal waves from the scope of this study. The proposed parameterizations are compared with limited field data to assess potential applicability of the proposed parameterizations to the field. It is also shown that the parameterization may be reduced to an Ri_g -based ones, provided that a simple relationship exists in the field between Fr_d^{-1} or Ri_g and the turbulent Reynolds number

$$Re_d = \frac{q^A}{\nu \epsilon}, \quad (5)$$

where ν is the molecular kinetic viscosity.

[9] This paper is organized as follows. Section 2 presents a theoretical background to introduce relationships used to constrain the proposed parameterizations. Section 3 briefly describes the data sets analyzed in this study. The parameterizations of turbulent quantities are developed in section 4. The results are compared to some field data in section 5, and used to develop Ri_g -based parameterizations in section 6. Implications of the results to hydrodynamic modeling and field data analysis are discussed in section 7, followed by brief conclusions.

2. Theoretical Background

[10] Following previous studies on homogeneous stably stratified shear flows, data analysis in this study is based on the standard equations of Turbulent Kinetic Energy (TKE) and (available) Turbulent Potential Energy (TPE). As in previous studies, mean flow is assumed unidirectional, and coordinates x , y , and z are taken in the longitudinal, transverse, and vertical directions, respectively. Velocity components, (u, v, w) , and density, ρ , are decomposed into mean and turbulent components; for example $u = \bar{u} + u'$, where the over bar denotes appropriate mean and the prime denotes turbulent fluctuation. Mean velocity, \bar{u} , and mean density, $\bar{\rho}$, are assumed to vary linearly with z , such that $\partial \bar{u} / \partial z = S$ and

$\partial\bar{\rho}/\partial z = -g^{-1}\bar{\rho}N^2$. Mixing is assumed to be so slow that N^2 may be assumed constant. Stratification is assumed to be due to either temperature or salt. Then, TKE and TPE equations are given by [e.g., *Rohr et al.*, 1988b; *Holt et al.*, 1992]

$$\frac{\partial E_K}{\partial t} = P - b - \varepsilon, \quad (6a)$$

$$\frac{\partial E_P}{\partial t} = b - \varepsilon_P, \quad (6b)$$

where t is the time, $E_K = q^2/2 = \overline{u_i' u_i'}/2$ is the TKE, $E_P = g^2 \bar{\rho}^2 (2\bar{\rho}^2 N^2)^{-1}$ is the TPE, $P = -\overline{u'w'}$ is the rate of turbulence production, $b = g\bar{\rho}^{-1}\overline{\rho'w'}$ is the turbulent buoyancy flux, $\varepsilon = \nu(\partial u_i'/\partial x_k)(\partial u_i'/\partial x_k)$ is the rate of TKE dissipation, $\varepsilon_P = g^2 \chi (2\bar{\rho}^2 N^2)^{-1}$ is the rate of TPE dissipation, $\chi = 2\kappa(\partial\rho'/\partial x_k)(\partial\rho'/\partial x_k)$ is the destruction rate of density variance ρ'^2 , and κ is the thermal diffusivity. Here, index notation, $(x_1, x_2, x_3) = (x, y, z)$ and $(u_1, u_2, u_3) = (u, v, w)$, is used for convenience, and the summation rule applies to repeated indices. Not only P and b but also ε_P provides a measure of mixing, because ε_P is an irreversible conversion rate of TPE to Background Potential Energy (BPE) [*Winters et al.*, 1995]. Note that ε_P used in this study is an experimental proxy for the conversion rate, because it must be referenced to stratification that has minimum potential energy attainable through adiabatic adjustments but it is difficult to do in laboratory experiments (and in the field [e.g., *Smyth et al.*, 2001]).

[11] In fully developed homogeneous stably stratified shear flows, turbulence properties, such as E_K , E_P , and $\overline{u'w'}$, grow or decay exponentially; however, a ratio of turbulence properties, such as $\overline{u'w'}/q^2$ and E_P/E_K , approaches a constant value, and the flow becomes dynamically self-similar (or self-preserving or structural equilibrium) [*Champagne et al.*, 1970; *Tavoularis and Karnik*, 1989; *Shih et al.*, 2000]. (Note that constant E_P/E_K implies equal relative growth rates of TKE and TPE; i.e., $E_K^{-1} \partial E_K / \partial t = E_P^{-1} \partial E_P / \partial t$.) Therefore, it is convenient to eliminate the variation due to change in turbulence intensity. Assuming exponentially growing or decaying turbulence and equal relative growth rates for TKE and TPE, (6a) and (6b) yield

$$\frac{1}{2}\gamma = -B_{13}\text{Sh}_d - \Gamma - 1, \quad (7a)$$

$$\frac{1}{2}\alpha\gamma = \Gamma - \Gamma_d, \quad (7b)$$

where the following nondimensional variables are introduced

$$-B_{13} = -\frac{\overline{u'w'}}{q^2} = \frac{P}{\varepsilon} \text{Sh}_d^{-1}, \quad \Gamma = \frac{b}{\varepsilon}, \quad \Gamma_d = \frac{\varepsilon_P}{\varepsilon}, \quad (8a)$$

$$\alpha = \frac{E_P}{E_K}, \quad \gamma = \frac{q^2}{\varepsilon E_K} \frac{\partial E_K}{\partial t} = \frac{q^2}{\varepsilon E_P} \frac{\partial E_P}{\partial t}. \quad (8b)$$

In the above equations, $B_{ij} = \overline{u_i' u_j'}/q^2 - \delta_{ij}/3$ (δ_{ij} is the Kronecker delta) are the normalized anisotropic components of the Reynolds stress, Γ is the variable often referred as

mixing efficiency in oceanography [e.g., *Osborn*, 1980; *Oakey*, 1985], α and Γ_d are the partition coefficients of turbulent energy and dissipation rate, respectively, and γ is the nondimensional exponential growth rate. Note that the assumption of equal relative growth rates (hence (7a) and (7b)) is found to hold for well-developed decaying shear flows (i.e., not in a self-similar state, and other nondimensional variables evolve in time) analyzed in this study. This assumption does not hold for the unsheared flows in general, but we may choose data points that satisfy the condition. The growth rate is usually normalized by S for shear flows and N for unsheared stratified flows [*Harris et al.*, 1977; *Itswire et al.*, 1986], but it is normalized here by ε/q^2 to make parameterizations applicable to both unsheared and unstratified cases.

[12] Some more relationships are useful to develop mixing parameterizations. The Ellison scale l_E , (isotropic version of) buoyancy scale l_B [*Peters et al.*, 1995], and Ozmidov scale l_O are defined as

$$l_E = -\frac{\bar{\rho}^2}{\partial\bar{\rho}/\partial z}^{1/2}, \quad l_B = \frac{q}{N}, \quad l_O = \left(\frac{\varepsilon}{N^3}\right)^{1/2}, \quad (9)$$

so the length scale ratios, l_E/l_d , l_E/l_B , and l_E/l_O , can be written as

$$\frac{l_E}{l_d} = \frac{l_E \varepsilon}{q^3} = \alpha^{1/2} \text{Fr}_d, \quad \frac{l_E}{l_B} = \alpha^{1/2}, \quad \frac{l_E}{l_O} = \alpha^{1/2} \text{Fr}_d^{-1/2}. \quad (10)$$

Normalized eddy viscosity ν_t and diffusivity κ_t are given by

$$\frac{\nu_t S^2}{\varepsilon} = -B_{13} \text{Sh}_d, \quad \frac{\kappa_t N^2}{\varepsilon} = \Gamma, \quad (11)$$

so the flux Richardson number $\text{Ri}_f = b/P$ and the turbulent Prandtl number $\text{Pr}_t = \kappa_t/\nu_t$ are expressed as

$$\text{Ri}_f = \frac{\Gamma}{-B_{13} \text{Sh}_d}, \quad \text{Pr}_t = \frac{\text{Ri}_g}{\text{Ri}_f} = \frac{-B_{13} \text{Fr}_d^{-2}}{\Gamma \text{Sh}_d}. \quad (12)$$

Note that there is another common definition $\text{Ri}_f = \Gamma/(\Gamma + 1)$ [e.g., *Rohr et al.*, 1984; *Ivey and Imberger*, 1991], but (12) is used in this study because it is more convenient in developing the parameterizations. Note also that $\text{Ri}_f \rightarrow \infty$ as $\text{Sh}_d \rightarrow 0$ with this definition, because $\text{Sh}_d = 0$ and $\Gamma = 0$ in unsheared stratified flows. However, Ri_f is usually considered to have an upper limit in shear flows. This is probably because there is a lower limit of Sh_d given by $(-B_{13})^{-1}$ ($= 6.25$ assuming $-B_{13} = 0.16$) in turbulence sustained by shear, which can be obtained by assuming $\gamma = \Gamma = 0$ in (7a).

3. Data Sets

[13] The results of previous laboratory and numerical experiments on (nearly) homogeneous stably stratified shear flows are compiled for this study (Table 1). Homogeneous unstratified shear flows and unsheared stratified flows are included as special cases of stratified shear flows. The data are classified into three categories: 'self-similar shear flows', 'decaying shear flows', and 'unsheared flows'. Homogeneous shear flows eventually develop to a self-similar stage, in which Sh_d approaches a narrow range of values around 10 provided that the Reynolds number is high. In unsheared

Table 1. Summary of Data Sets Analyzed in This Study

Article	Type ^a	Source	Notes
<i>Self-Similar Shear Flows</i>			
<i>Tavoularis and Corrsin</i> [1981]	Wind tunnel	Tables 4 and 6	$x/h = 11$; χ estimated from (A1) ^b
<i>Rogers and Moin</i> [1987]	DNS	Web repository ^c	$St = 12, 14, \dots$; Runs: u, w, x
<i>Rohr et al.</i> [1988a]	Water channel	Tables 1 and 2 of <i>Tavoularis and Karnik</i> [1989]	$St \geq 8^d$; $\overline{v^2} = (27/73)(\overline{u^2} + \overline{w^2})$ is assumed; χ estimated from (A1) ^{e,f}
<i>Rohr et al.</i> [1988b]	Water channel	Appendix 2 of <i>Rohr</i> [1985]	
<i>Tavoularis and Karnik</i> [1989]	Wind tunnel	Tables 1 and 2	Cases A ~ K
<i>Kaltenbach et al.</i> [1994]	LES (Pr = 1)	Table 1	$Ri_g = 0, 0.13, 0.25$; $St = 8, 10, 12$
<i>Shih et al.</i> [2000, 2005]	DNS (Pr = 0.72)	Database from authors	Runs: bg, bh, bi, bj, bk, bl, bo, bp, bq, br, bu, bv, bw, bx, bz, ek, el, em, fa, fb, fc, fd, fe, ff, fg, fh, fl, fp, fz; $St = 9, 11, \dots^g$
<i>Decaying Shear Flows</i>			
<i>Stillingner</i> [1981]	Water channel	Table B-11 ~ 13	$x/M = 20, 30^d$; $\overline{v^2} = (27/73)(\overline{u^2} + \overline{w^2})$ assumed
<i>Kaltenbach et al.</i> [1994]	LES (Pr = 1)	Table 1	$Ri_g = 0.5, 1.0$; $St = 8, 10, 12$
<i>Shih et al.</i> [2000, 2005]	DNS (Pr = 0.72)	Database from authors	Runs: ba, bb, bc, bd, en, eo, fi, fo, fq, fr; $St = 6 \sim 7, 8 \sim 9, \dots$ for b series, $5 \sim 7, 7 \sim 9, \dots$ for the rest ^h
<i>Unsheared Flows</i>			
<i>Itsweire et al.</i> [1986]	Water channel	Table 2	$x/M \geq 20^d$; $\overline{v^2} = \overline{u^2}$ assumed
<i>Lienhard and van Atta</i> [1990]	Wind tunnel	Tables 1 ~ 4	$x/M \geq 20^i$; $\overline{v^2} = \overline{u^2}$ assumed

^aStratifying agent is temperature for all the wind tunnel experiments and salt for all the water channel experiments.

^b $Ri_g = 1.37 \times 10^{-4}$ is calculated from the values in Table 4 of *Tavoularis and Corrsin* [1981].

^cSee <http://www.efluids.com/efluids/databases/agard.html>.

^dOnly data points corresponding to ‘overturning motion’ that satisfy $\varepsilon/(\nu N^2) > 15$ (but $\varepsilon/(\nu N^2) > 21$ for $M = 0.0381$ m cases of *Itsweire et al.* [1986]) are used.

^eHere χ is estimated only when $\overline{\rho^2}$ is approximately constant in time, as done in the paper.

^fHere $\overline{\rho^2}$ is divided by 2 for reasons explained in Appendix A.

^gResults just before reaching odd values of St are used to minimize alias errors due to remeshing.

^hData are averaged over specified intervals.

ⁱData during ‘stratification overshoot’ are excluded.

flows, turbulence decays exponentially but the dynamic balance does not approach a self-similar state. Such decaying behavior has also been noticed in high Ri_g shear flows by *Kaltenbach et al.* [1994], and the DNS database of *Shih et al.* [2000, 2005] supports their observation. Contrary, water channel experiments by *Stillingner* [1981] indicate that high Ri_g flows approach a self-similar state with terminal Sh_d being close to 10. The characteristics of fully developed conditions in strongly stratified shear flows is unclear at this stage; however, it is clear that turbulence decays exponentially and α becomes constant in time, so these cases are included in this study and classified as ‘decaying shear flows’.

[14] The following general rules are applied to make the data sets as homogeneous as possible. High Reynolds number cases are chosen to minimize viscous effects. For the self-similar shear flows, only data at large nondimensional time ($St \geq 8$) are used so that the flow is as close to a self-similar state as possible. For the decaying stratified shear flows, data points in well-developed conditions (with constant α) are used. This corresponds to $x/M \geq 20$ (M is the spacing between rods or grids used to generate turbulence) for water channel experiments by *Stillingner* [1981] and $St \geq 5$ for DNS by *Shih et al.* [2000, 2005]. For unsheared flows, only data points that have approximately equal (within 30%) growth rates of TKE and TPE are used due to an assumption made in the theoretical development. Data points near the grid ($x/M < 20$) are excluded since the flow has not adjusted to background stratification [*Lienhard and van Atta*, 1990]. It should be noted that in strongly stratified flows, turbulence properties, particularly b , show an oscillatory behavior with a period close to π/N [*Gerz et al.*, 1989; *Lienhard and van Atta*, 1990]. Large scatter associated with such an

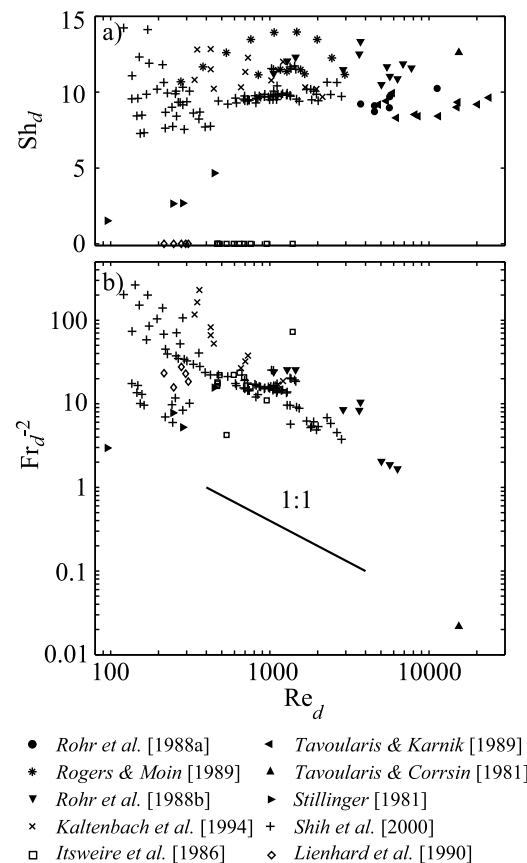


Figure 1. Scatterplots of (a) Re_d versus Sh_d and (b) Re_d versus Fr_d^{-2} . In Figure 1b, solid line indicates slope of 1.

Table 2. Summary of Constraints Used to Develop Fr_d^{-1} Dependence of $f_1 \sim f_3^a$

Physical Constraint	Constraint on $f_1 \sim f_3$
<i>Limit of Low Fr_d^{-1}</i>	
l_E/l_d constant	$f_2 \propto Fr_d^{-2}$
Pr_t constant	$f_3 \propto Fr_d^{-2}$
<i>Limit of High Fr_d^{-1}</i>	
α constant	$f_2 \propto Fr_d^0$
Ri_j constant ($Pr_t \propto Ri_g$)	$f_3 \propto Fr_d^0$
<i>All Range of Fr_d^{-1}</i>	
$-B_{13} > 0$	$0 < f_1$
$0 \leq Ri_j < \infty, 0 \leq \alpha < \infty$	$0 \leq f_3 \leq f_2/f_1$

^aDefined in Table 3.

oscillation is minimized as follows. For DNS experiments, nondimensional parameters are calculated and then averaged in time. For water channel experiments, only data points that satisfy the minimum $\varepsilon/(\nu N^2)$ criteria used by *Itsweire et al.* [1986] and *Ivey and Imberger* [1991] are retained. For wind tunnel experiments by *Lienhard and van Atta* [1990], data points corresponding to the ‘stratification overshoot’ are excluded. Further details on processing of each data set are given in Appendix A.

[15] The ranges of Re_d , Sh_d , and Fr_d^{-1} covered by the data sets are shown in Figure 1. Sh_d ranges from 8 to 15 in the self-similar shear flows, but reaches as low as ≈ 3 in the decaying shear flows (Figure 1a). Unfortunately, there is a strong correlation between Re_d and Fr_d^{-1} (Figure 1b), and parameterizations based on Fr_d^{-1} may include systematic Re_d effects. This is elaborated in the discussion. Since the initial Reynolds number is limited in the experiments, the decaying shear flows and unsheared flows unavoidably have lower Re_d , and the results are not free from Reynolds number effects, as shown later.

4. Parameterizing Nondimensional Turbulent Quantities

[16] The goal of this study is to parameterize the nondimensional turbulent fluxes, $P/\varepsilon = -B_{13}Sh_d$ and $b/\varepsilon = \Gamma$, and the nondimensional conversion rate of TPE to BPE, Γ_d , in terms of Sh_d and Fr_d^{-1} . Initially, attempts were made to parameterize these parameters directly, but such attempts failed. One reason is the difficulty in distinguishing Sh_d and Fr_d^{-1} dependences due to large scatter of buoyancy flux b . Another reason is that various nondimensional variables introduced in section 2 are related to each other, and careless parameterizations of $-B_{13}$, Γ , and Γ_d result in unphysical behaviors of other variables. In this study, it is decided to exploit the fact that only three independent functions $f_1 \sim f_3$ are required to quantify the five nondimensional variables in (8a) and (8b), constrained by equations (7a) and (7b). We may choose to parameterize variables that have clearer dependence on Sh_d and Fr_d^{-1} with less scatter. By taking an approach similar to *Munk and Anderson* [1948], we can also constrain parameterizations by (1) known behaviors of l_E/l_d , α , Pr_t , and Ri_j ; (2) positiveness of Ri_j , α , and Γ_d ; and (3) the governing equations (7a) and (7b). The three fitted functions then provide five variables in (8a) and (8b).

[17] The details of the choice of $f_1 \sim f_3$ and fitting procedure are explained in the following. Readers who are not interested in the details may go to section 4.4; the summary of constraints and resulting parameterizations are given in Tables 2 and 3, respectively.

4.1. Choosing $f_1 \sim f_3$

[18] We need to set $f_1 = -B_{13}$ because $-B_{13}$ is the only parameter required in unstratified shear flows. In this study, f_2 and f_3 are related to Γ_d and α since b has large scatter and growth rates are less available than q^2 , $\overline{\rho'^2}$, ε , and ε_p . We choose $f_2 = \Gamma_d$ because Γ_d has a clearer trend than α , and it is available from common microstructure measurements. The choice of f_3 needs some care. This can be shown by

$$Ri_f = \frac{1}{1 + \alpha} \left(\frac{\Gamma_d - \alpha}{-B_{13}Sh_d} + \alpha \right), \quad (13)$$

which is derived by deleting γ from (7a) and (7b). Since $-B_{13}$ decreases rapidly with increasing Fr_d^{-1} (shown later)

Table 3. Summary of Proposed Parameterizations in Terms of $Sh_d = q^2 S/\varepsilon$ and $Fr_d^{-1} = q^2 N/\varepsilon^a$

Variable	Expression
<i>Derived Constants</i>	
C_2^W	$\frac{-B_{13,0}}{Sh_{d0}Pr_{t0}} - (-B_{13,0}Sh_{d0} - 1)(l_E/l_d)_0^2$
C_2^S	α_0
C_3^W	$\frac{1}{Sh_{d0}Pr_{t0}} - Sh_{d0}(l_E/l_d)_0^2$
C_3^S	$((1 + \alpha_0)Ri_{j0} - \alpha_0)Sh_{d0}$
<i>Fitted Variables</i>	
$f_1 = -B_{13}$	$-B_{13,0} \exp(-C_1 Fr_d^{-n_1})$
$f_2 = \Gamma_d$	$((C_2^W g_2^W Fr_d^{-2})^{-n_2} + (C_2^S g_2^S)^{-n_2})^{-1/n_2}$, $g_2^W = \exp(-A_2^W (Sh_d - Sh_{d0}))$
f_3	$((C_3^W g_3^W Fr_d^{-2})^{-n_3} + (C_3^S g_3^S)^{-n_3})^{-1/n_3}$, $g_3^W = \exp(-A_3^W (Sh_d - Sh_{d0}))$
<i>Derived Variables</i>	
P/ε	$f_1 Sh_d$
$\Gamma = b/\varepsilon$	$f_1 \frac{(f_2 - f_1 f_3) Sh_d + f_3}{1 + f_2 - f_1 f_3}$
Ri_f	$\frac{f_2 - f_1 f_3 + f_3 Sh_d^{-1}}{1 + f_2 - f_1 f_3}$
Pr_t	$\frac{1 + f_2 - f_1 f_3}{f_2 - f_1 f_3 + f_3 Sh_d^{-1}} Sh_d^{-2} Fr_d^{-2}$
$\alpha = (l_E/l_d)^2$	$f_2 - f_1 f_3$
l_E/l_d	$(f_2 - f_1 f_3)^{1/2} Fr_d$
l_E/l_0	$(f_2 - f_1 f_3)^{1/2} Fr_d^{-1/2}$
γ	$2 \frac{f_1 Sh_d - 1 - f_2}{1 + f_2 - f_1 f_3}$

^aFollowing fitting parameters are obtained for data sets in Table 1 with a reference shear number of $Sh_{d0} = 10$: $(l_E/l_d)_0 = 0.09$, $Pr_{t0} = 0.8$, $\alpha_0 = 0.35$, $Ri_{j0} = 0.3$, $(n_1, n_2, n_3) = (3, 2, 2)$, $(A_2^W, A_2^S, A_3^S) = (0.2, 0.2, 0.07)$, and $C_1 = 0.005$. Here $-B_{13,0} = 0.16$ is taken from *Rohr et al.* [1988b] and *Tavoularis and Karnik* [1989]. The parameterizations are valid for $Sh_d = 0 \sim 15$, provided that the flow have approximately equal growth rates of TKE and TPE.

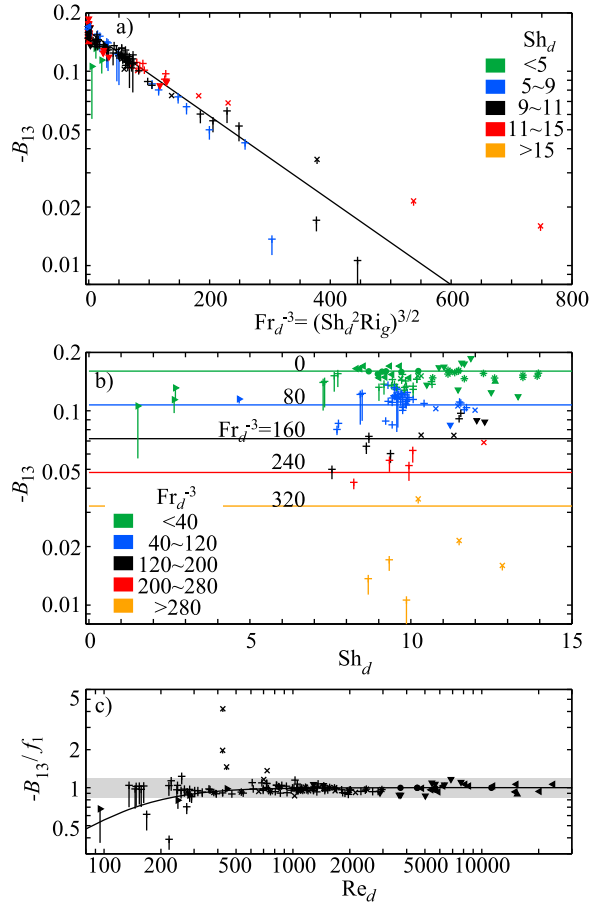


Figure 2. Dependence of $-B_{13}$ on (a) Fr_d^{-3} , (b) Sh_d , and (c) Re_d . In Figures 2a and 2b, color shows range of Sh_d and Fr_d^{-3} , respectively. In Figure 2c, $-B_{13}$ is normalized by f_1 , indicating fitting errors ($= 1$ for perfect fit). Shading indicates fitting within a factor of 1.2. Since $-B_{13}$ clearly decreases with Re_d , Re_d effects are corrected by the curve shown in the panel (analytical expression is $(1 + (150Re_d^{-1})^2)^{-1/2}$). The lower ends and upper ends (with symbols) of vertical lines show values before and after this correction, respectively. Solid lines show proposed parameterization. See Table 3 for a definition of f_1 . See Figure 1 for symbols.

and $\Gamma_d - \alpha$ can be negative, one must be careful to assure finiteness (for $Sh_d > 0$) and positiveness of Ri_f . It is most convenient to set $\Gamma_d - \alpha$ being proportional to $-B_{13}$, so that Ri_f remain finite for high Fr_d^{-1} . Therefore, we set

$$f_3 = (\Gamma_d - \alpha)/f_1 \quad (> 0). \quad (14)$$

4.2. Constraints on f_2 and f_3

[19] The Fr_d^{-1} dependence of f_2 and f_3 can be determined from the following four constraints. First, it is known that $l_E/l_d = l_E \varepsilon/q^3$ is approximately constant for active turbulence that is only weakly affected by stratification [Ivey and Imberger, 1991; Schumann and Gerz, 1995], and (10) implies $\alpha \propto Fr_d^{-2}$ for low Fr_d^{-1} . Second, in stratified turbulence, l_E is commonly considered to grow up to l_O (within a factor of $O(1)$) from laboratory experiments

[Stillinger et al., 1983; Itsweire et al., 1986; Rohr et al., 1988b] and numerical experiments [Smyth et al., 2001; Shih et al., 2005]. However, the data analyzed in this study suggests that l_E grows up to l_B (shown later). We choose $l_E/l_B \sim$ constant based on available data, and (10) implies $\alpha \propto Fr_d^0$ for high Fr_d^{-1} . Since $f_1 \ll 1$ for high Fr_d^{-1} , (14) then implies $f_2 = \Gamma_d \propto Fr_d^0$. Third, Ri_f has to be significantly less than one for shear driven flows, and (13) implies $f_3 \propto Fr_d^0$ for high Fr_d^{-1} using $\alpha \propto Fr_d^0$. Fourth, Pr_t becomes constant under weak stratification [e.g., Shih et al., 2005; Zilitinkevich et al., 2008]. From (12), (13), and (14), Pr_t can be written as

$$Pr_t = \frac{1 + \alpha}{f_3 Sh_d^{-1} + \alpha} Sh_d^{-2} Fr_d^{-2}. \quad (15)$$

For low Fr_d^{-1} , we have $\alpha \propto Fr_d^{-2}$, so constant Pr_t (independent of Fr_d^{-1}) requires $f_3 \propto Fr_d^{-2}$. Then, this relation, $\alpha \propto Fr_d^{-2}$, and (14) require $f_2 = \Gamma_d \propto Fr_d^{-2}$ for low Fr_d^{-1} . In order to have $\alpha > 0$, there is also a constraint

$$f_2 > f_1 f_3 \quad (\geq 0). \quad (16)$$

4.3. Details of Fitting Process

[20] First, f_1 is determined from $-B_{13}$ (Figure 2). The data show clearly the suppression of $-B_{13}$ by stratification (Figure 2a). The Fr_d^{-1} dependence is well described by log ($f_1 \propto Fr_d^{-3}$). Low Sh_d and high Fr_d^{-1} data appear to show some Sh_d dependence, but this is not parameterized considering the uncertainty. Figure 2c shows $-B_{13}/f_1$, which indicates a fitting error, as a function of Re_d . Unfortunately, there is a bias at low Re_d . In this study, the bias is corrected using the curve shown in the figure. After this Re_d correction, the parameterization agrees with most of the data within a factor of 1.2.

[21] Second, the functional form of f_2 is determined as follows. Γ_d increases with increasing Fr_d^{-1} to a maximum value, and Sh_d dependence appears only in the low Fr_d^{-1} regime (Figures 3a and 3b). Extrapolation of the slope for low Sh_d to $Sh_d = 0$ agrees with unshered cases within the scatter, indicating that shered and unshered cases can be treated together (Figure 3b). For fitting, a functional form $f_2 = C_2 Fr_d^m$ ($m = -2$ or 0) is assumed from the constraints discussed above. The fitting parameter C_2 in the limits of low and high Fr_d^{-1} (referred as C_2^W and C_2^S , respectively) are initially obtained separately for a reference shear number of $Sh_{d0} = 10$, and the functions at the two limits are interpolated later to get a function for a full range of Fr_d^{-1} (black line in Figure 3a). Then, Sh_d dependence is introduced by multiplying C_2^W by an exponential function of Sh_d . Since uncertainty is large in this fitting, a relatively small fitting parameter is chosen, not to exaggerate Sh_d dependence. For unshered cases, there is a clear offset between data points from salt-stratified water channel experiments by Itsweire et al. [1986] and temperature-stratified wind tunnel experiments by Lienhard and van Atta [1990]. This may be due to the difference of (molecular) Prandtl number $Pr = \nu/\kappa$, but such a difference does not appear in the analyzed shear flow data. In this study, f_2 is fitted between the two data sets. There is no clear Re_d dependence, and most data points lie within a factor of 1.2 from the

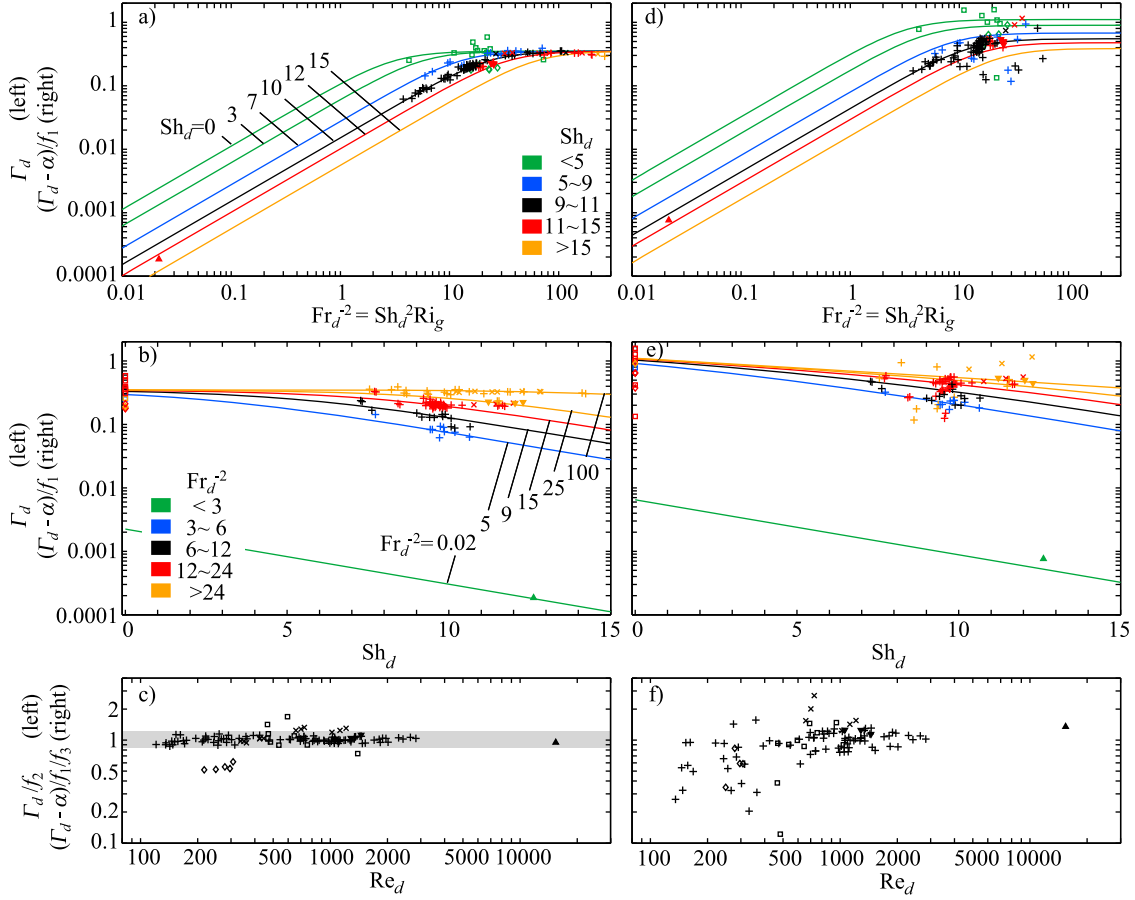


Figure 3. Dependence of (a–c) Γ_d and (d–f) $(\Gamma_d - \alpha)/f_1$ (for $\text{Fr}_d^{-2} < 70$) on Fr_d^{-2} (Figures 3a and 3d), Sh_d (Figures 3b and 3e), and Re_d (Figures 3c and 3f). In Figures 3a and 3d, color shows range of Sh_d in the same scale, and in Figures 3b and 3e that of Fr_d^{-2} . In Figures 3c and 3f, Γ_d and $(\Gamma_d - \alpha)/f_1$ are normalized by f_2 and f_3 , respectively, indicating fitting errors ($= 1$ for perfect fit). In Figure 3c, shading indicates fitting within a factor of 1.2. Solid lines show proposed parameterizations with common Sh_d for Figures 3a and 3d and common Fr_d^{-2} for Figures 3b and 3e. See Table 3 for a definition of f_2 and f_3 . See Figure 1 for symbols.

parameterization (Figure 3c). Note that Sh_d dependence is necessary to achieve such a good fit.

[22] Third, f_3 is determined by plotting $(\Gamma_d - \alpha)/f_1$, although this variable unavoidably has large scatter particularly at high Fr_d^{-1} (Figures 3d and 3e). Hence, only data points for $\text{Fr}_d^{-2} < 70$ are used for this fitting. $(\Gamma_d - \alpha)/f_1$ has Sh_d and Fr_d^{-1} dependences similar to Γ_d . A difference is that $(\Gamma_d - \alpha)/f_1$ has a weak Sh_d dependence at high Fr_d^{-1} (Figure 3e). This can be seen from unsheared flows having larger values than shear flows on average, despite large scatter in both cases. $(\Gamma_d - \alpha)/f_1$ tends to be smaller for low Re_d (Figure 3f), which is probably related to Re_d effects on vertical velocity (Appendix B). Re_d effects are not corrected due to the unclear trend, but the fitting aims larger values within the scatter. f_3 is parameterized following the similar process used to determine f_2 , except that different Sh_d dependence is applied to the low and high Fr_d^{-1} regimes. Fitting error is large due to noisy nature of the variable and the Re_d effects (Figure 3f), but parameterized α is within a factor of 1.4 from most of the data (Figure A1). Note that including Sh_d dependence clearly improves the fit for low Fr_d^{-1} (Figure 4c).

[23] Having constructed $f_1 \sim f_3$, other nondimensional variables can be derived using (7a) and (7b), as summarized in Table 3. To calculate Γ , γ is derived by adding two equations in (7a) and (7b), and substituting the resulting γ back into (7a) and (7b). Taking the limits of low and high Fr_d^{-1} , we may relate fitting parameters C_2^W , C_2^S , C_3^W , and C_3^S to more physically meaningful variables using the following relationships: For low Fr_d^{-1}

$$(l_E/l_d)^2 \sim C_2^W - (-B_{13,0})C_3^W, \text{Pr}_t \sim \frac{\text{Sh}_d^{-2}}{C_2^W + C_3^W(\text{Sh}_d^{-1} - (-B_{13,0}))}, \quad (17a)$$

and for high Fr_d^{-1}

$$\alpha \sim C_2^S, \quad \text{Ri}_f \sim \frac{C_2^S + C_3^S \text{Sh}_d^{-1}}{1 + C_2^S}, \quad (17b)$$

where $-B_{13,0}$ is $-B_{13}$ at $\text{Fr}_d^{-1} = 0$. These relationships are used to calculate C_2^W , C_2^S , C_3^W , and C_3^S from limiting (constant) values of l_E/l_d and Pr_t at low Fr_d^{-1} , and α and Ri_f at high Fr_d^{-1} with a reference Sh_d of 10 (Figure 4 and Table 3).

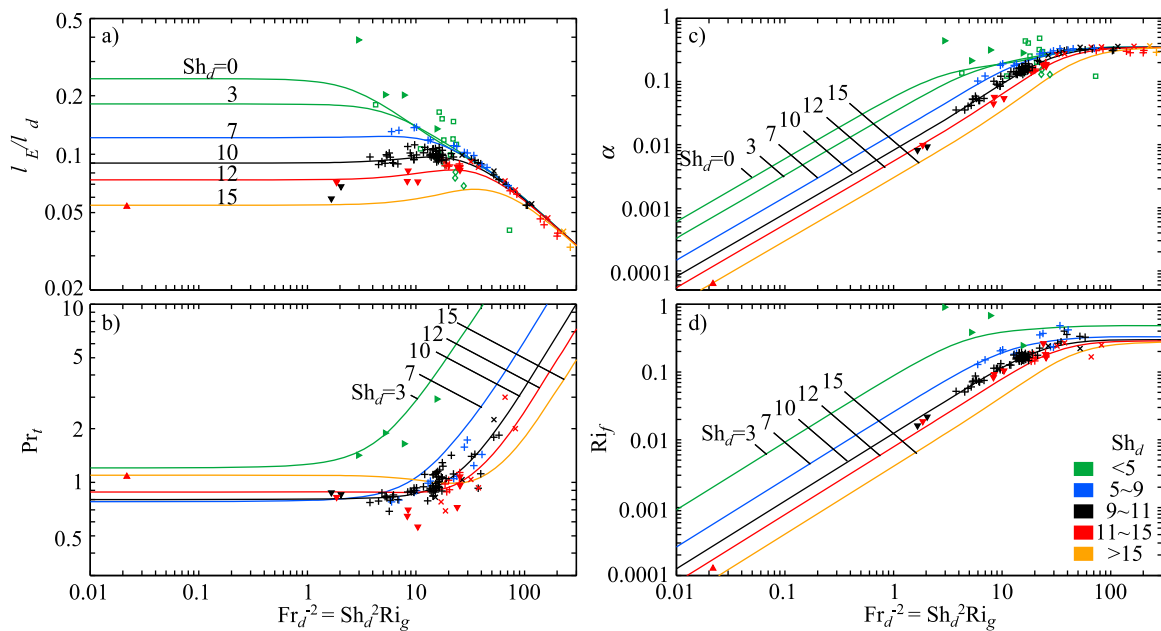


Figure 4. Fr_d^{-2} and Sh_d dependence of (a) l_E/l_d , (b) Pr_b , (c) α , and (d) Ri_f . Colors show range of Sh_d in the same scale, and solid lines show proposed parameterizations (Table 3). In Figures 4b and 4d, only data satisfying $P > 0$ and $b > 0$ are plotted. See Figure 1 for symbols.

The parameter set satisfies (16). Due to the scatter of data points within a data set, different trend or bias between data sets, and Re_d effects, fitting coefficients were obtained visually only for the nearest first digit, unless a second digit of 5 is required to eliminate clear and large bias.

4.4. Proposed Parameterizations

[24] The proposed parameterizations for nondimensional momentum flux P/ε and buoyancy flux $\Gamma = b/\varepsilon$ are given in Table 3. The suppression of turbulence production by stratification is parameterized well, and the parameterization of b/ε captures the trend in the data (see below), considering the large scatter (Figure 5). The valid range of Sh_d is 0 ~ 15 from the available range of Sh_d , but note that they have limited applicability to unsheared stratified flows because of the assumption of equal relative growth rates for TKE and TPE.

[25] A new result in the proposed parameterizations is the explicit parameterization of Sh_d dependence of b/ε . The data shows that b/ε has a peak at moderate Fr_d^{-1} , and the location shifts toward higher Fr_d^{-1} with increasing Sh_d (Figures 5c and 5e). b/ε is larger for lower Sh_d when Fr_d^{-1} is low (Figures 5c and 5d), but larger for higher Sh_d when Fr_d^{-1} is high (Figures 5e and 5f). The proposed parameterization captures these behaviors. It also predicts a maximum at moderate Sh_d , but this could not be confirmed due to the scarcity of data for high Sh_d .

[26] The measured and parameterized Γ_d , l_E/l_d , Pr_b , α , and Ri_f are compared in Figures 3a–3c and 4. They agree well, except that the parameterizations underestimate l_E/l_d and α from Stillinger [1981]. This is caused by the lack of Γ_d from Stillinger [1981] in the fitting process. However, it is also likely that the data points from Stillinger [1981] are biased

high due to Re_d effects on vertical velocity (Appendix B). The variations of Sh_d and Fr_d^{-1} cause comparable variations in l_E/l_d . For the other variables, variations due to Fr_d^{-1} are dominant, but the increase of Sh_d still causes significant decreases of Γ_d , α , and Ri_f for low Fr_d^{-1} , and Pr_b for high Fr_d^{-1} .

5. Some Comparisons With Field Data

[27] Since the proposed parameterizations are obtained based on laboratory and numerical experiments, it is important to see how the proposed parameterizations compare with field data. Due to limited availability of field data for this study, the purpose here is to show that the proposed parameterizations are comparable with field data, so that detailed comparison in the future is worthwhile.

[28] For the comparisons, we need to relate l_E , used in the proposed parameterizations, and the Thorpe scale l_T , commonly used in the field data analysis. *Itsweire et al.* [1986] and *Itsweire et al.* [1993] found $l_T/l_E = 1.2$ and 0.8 in laboratory and DNS experiments, respectively, whereas *Moum* [1996b] reports $l_T/l_E = 1.7$ from thermocline in a midlatitude ocean.

[29] The shear number Sh_d is an important parameter used in this study, but Sh_d in the field is not reported in previous studies. Here, Sh_d is estimated from correlations between turbulent quantities from a thermally stratified lake by *Saggio and Imberger* [2001] and from the equatorial Pacific by *Peters et al.* [1995]. *Saggio and Imberger* [2001] suggests $\varepsilon/(\nu N^2) = 5.3 Ri_g^{-3/2}$ under weak stratification for their data. Combining this relation and (4) leads to $Fr_d = 5.3^{-1/3} Sh_d^{-1} (\varepsilon/(\nu N^2))^{1/3}$. The slope of the data shown in Figure 22b of *Saggio and Imberger* [2001]

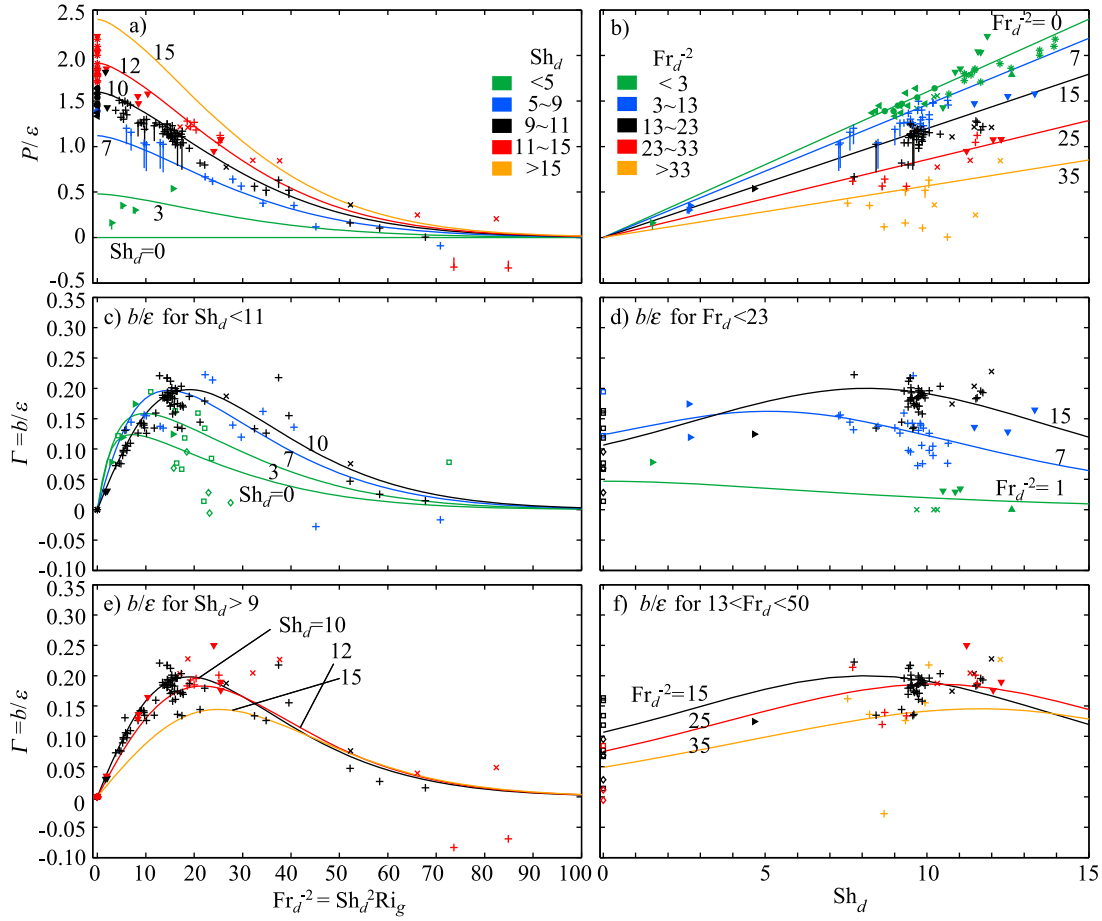


Figure 5. Comparison of measured and parameterized (a and b) P/ε and (c–f) b/ε . For ease of distinguishing Sh_d dependence, Figures 5c and 5e show b/ε for $Sh_d < 11$ and > 9 , respectively, and Figures 5d and 5f for $Fr_d^{-2} < 23$ and > 13 . In Figures 5a and 5b, the lower ends and upper ends (with symbols) of vertical lines show, respectively, values before and after Re_d correction shown in Figure 2c. Colors show range of Sh_d in Figures 5a, 5c, and 5e in the same scale and that of Fr_d^{-2} in Figures 5b, 5d, and 5f. Solid lines show proposed parameterizations (Table 3). See Figure 1 for symbols.

appears to agree with this dependence. Visual fitting gives $Fr_T = (0.2 \sim 0.3) \times (\varepsilon/(\nu N^2))^{1/3}$. Using $l_E/l_d = 0.3$ from the paper, and $l_T/l_E = 1$ due to lack of the data from lakes, we get $Sh_d = 6 \sim 10$. Figure 11a of *Peters et al.* [1995] appears to show $Fr_T \propto Ri_g^{-1/2}$ for low Ri_g , although scatter is large and the correlation is weak (Figure 6a). Using the parameters obtained from laboratory and numerical experiments and $l_T/l_E = 1.7$ from an ocean, the proposed parameterization predicts magnitude that is about in the middle of the scatter. Shear number dependence is unfortunately small, but $Sh_d = 5 \sim 15$ are within the scatter of the data. These limited cases suggest that Sh_d in the experiments are comparable with estimates from the field.

[30] Since f_2 and f_3 are constrained through l_E/l_d , Pr_r , α , and Ri_f , these parameters are compared to selected field data (Table 4). Overall, the parameters are comparable between laboratory and numerical experiments and the field, considering relatively large variation of l_E/l_d with Sh_d (Figure 4a). A few points are worth noting here. *Peters et al.* [1995]

report an anomalous result, $l_E/l_d = 4.4$, in the equatorial Pacific, and the reason is unclear. *Moum* [1996b] reports constant l_E/l_d and $l_E/l_B (= \alpha^{1/2})$, and Figures 4a and 4c suggests that it is possible at fixed Fr_d^{-2} . *Moum* [1996b] reports $\varepsilon = 0.73Nw^2$, which leads to $Fr_d^{-2} \approx 17$ assuming isotropy. This Fr_d^{-2} suggests that l_E/l_d and α found by *Moum* [1996b] are lower than their limiting values at low and high Fr_d^{-1} , respectively. Considering these, the comparisons suggest that f_2 and f_3 are not very different in laboratory and numerical experiments and in the field. Good estimates of momentum and buoyancy fluxes in the field are required to constrain f_1 for high Fr_d^{-1} because it determines how quickly $-B_{13}$ and Γ decreases with increasing stratification.

6. Reduction to Ri_g -Based Parameterizations

[31] By taking advantage of (4), the proposed parameterizations may be reduced to Ri_g -based parameterizations, that are useful in idealized studies and numerical models designed for computationally demanding runs, such as general

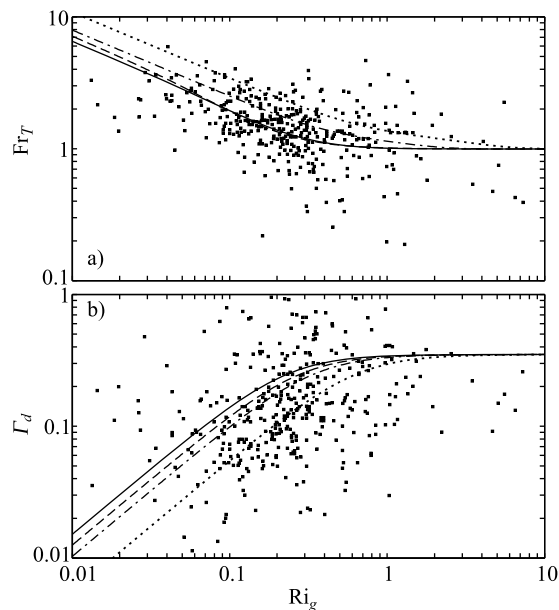


Figure 6. Comparisons of (a) Fr_T and (b) Γ_d between proposed parameterizations and field data from equatorial Pacific by *Peters et al.* [1995]. For field data, Fr_T is calculated from Fr_t using $l = 1.67l_T$ (for details see *Peters et al.* [1995]). Proposed parameterizations for Fr_E are calculated using l_E/l_d in Table 3 and then converted to Fr_T using $l_T/l_E = 1.7$, suggested by *Moum* [1996b]. Dotted, dash-dotted, solid, and dashed lines show proposed parameterization at $Sh_d = 0, 5, 10$, and 15 , respectively, using fitting coefficients from laboratory and numerical experiments (Table 3). Although scatter is large for Γ_d , there is statistically significant increase of Γ_d with increasing Ri_g for low Ri_g [*Peters et al.*, 1995].

circulation models [e.g., *Large et al.*, 1994]. To obtain actual eddy viscosity and diffusivity, turbulence intensity must be specified by site-specific field data because the proposed parameterizations are made independent of turbulence intensity, and because it varies by orders of magnitude in the

field. Taking an approach similar to *Shih et al.* [2005], (11) can be written as

$$\frac{\nu_t}{\nu} = -B_{13} Sh_d^{-1} Re_d, \quad (18a)$$

$$\frac{\kappa_t}{\kappa} = Pr \Gamma Fr_d^2 Re_d. \quad (18b)$$

Note that ν_t and κ_t are independent of ν and κ because ν and κ appearing in the denominators cancel using $Re_d = q^4/(\nu\varepsilon)$ and $Pr = \nu/\kappa$. However, ν and κ are retained in the above equations because the measure of turbulence intensity are usually reported in nondimensional form, such as $\varepsilon/(\nu N^2)$. Now, some field data support a monotonic relationship between Re_d and Ri_g . For low Ri_g , *Saggio and Imberger* [2001] suggest $\varepsilon/(\nu N^2) \propto Ri_g^{-3/2}$ based on microstructure measurements in the metalimnion of a stratified lake, and data from estuaries by *Peters* [1997] and *Stacey et al.* [1999] appear to support this relationship up to $Ri_g \approx 10$. Using this relationship, $\varepsilon/(\nu N^2) = Sh_d^{-2} Ri_g^{-1} Re_d$, and the assumption of constant Sh_d yield

$$Re_d = Re_{d0} \left(\frac{Ri_g}{Ri_{g0}} \right)^{-1/2}, \quad (19)$$

where (Ri_{g0}, Re_{d0}) are a set of reference values. Combining (18a), (18b), and (19) assuming constant Sh_d yields Ri_g -based parameterizations.

[32] Figure 7 shows the functional forms for Lake Kinneret, Israel, using $Sh_d = 10$ and $(Ri_{g0}, Re_{d0}) = (0.1, 600)$, estimated from Figure 19 of *Saggio and Imberger* [2001]. The proposed parameterization for κ_t/κ lies within the range of measured eddy diffusivity (i.e., directly measured turbulent buoyancy flux divided by N^2) in the lake by *Yeates* [2008]. Considering the assumptions made in this calculation, this result is encouraging. Compared to the data, parameterized κ_t decreases more rapidly with increasing Ri_g , suggesting that f_1 might decrease more slowly with increasing Fr_d^{-1} in the field. Figure 7 provides further support that

Table 4. Comparison of Parameter Values Used in the Parameterizations With Selected Field Data

Article	Location	$\frac{l_E}{l_d}$	Pr_t	$\alpha = \left(\frac{l_E}{l_d}\right)^{2a}$	Γ_d	$Ri_f = \frac{b}{P}$
This study	—	0.05 ~ 0.25	>0.8	<0.35	<0.35	<0.3
<i>Oakey</i> [1982, 1985]	Rockwall Trough	—	—	—	0.26	—
<i>Gargett and Moum</i> [1995]	Haro Strait	—	—	—	0.24	—
<i>Peters et al.</i> [1995]	Equatorial Pacific (0°, 140° W)	4.4 ^b	—	0.16 ^b	0.14 ^c	—
<i>Moum</i> [1996a, 1996b]	NE Pacific (39°N, 135°15'W)	0.08 ^{d,e}	—	0.12 ^{b,d}	0.3 ~ 0.4	—
<i>Ruddick et al.</i> [1997]	NE Atlantic (24~27°N, 28~36°W)	—	—	—	0.14 (fall), 0.22 (spring)	—
<i>Ravens et al.</i> [2000]	Lake Baikal	—	—	—	0.16	—
<i>Etemad-Shahidi and Imberger</i> [2001]	Lake Biwa and Lake Kinneret	0.46 ^f	—	—	—	—
<i>Saggio and Imberger</i> [2001]	Lake Kinneret	0.30 ^{f,g}	0.75	—	—	<0.19

^aNote that $\alpha \approx \Gamma_d$ at high Fr_d^{-1} in the proposed parameterizations.

^bAssuming $l_T/l_E = 1.7$ from NE Pacific Ocean [*Moum*, 1996b].

^cMedian value. Increases with increasing stratification and reaches ≈ 0.2 under strong stratification (see Figure 6).

^dLimiting value at high Fr_d^{-1} may be larger (see text).

^eAssuming isotropy ($3w'^2 = q^2$), as done by *Moum* [1996a, 1996b].

^fAssuming $l_T/l_E = 1.0$ due to lack of data from lakes.

^gLimiting value under weak stratification.

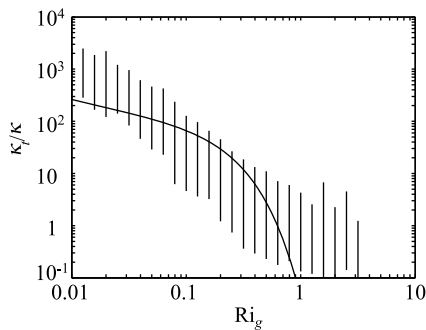


Figure 7. Normalized eddy diffusivity predicted by Ri_g -based parameterization (18a), (18b), and (19) for Lake Kinneret. $Sh_d = 10$ is assumed, and $(Ri_{g0}, Re_{d0}) = (0.1, 600)$ is estimated from Figure 19 of *Saggio and Imberger* [2001]. Other fitting coefficients are from laboratory and numerical experiments (Table 3). Vertical bars show measured eddy diffusivity in the lake by *Yeates* [2008]. Bar range shows eddy diffusivity that encompasses 66% of the dissipation observations. Note that comparison becomes difficult at the low end of Ri_g because *Yeates* [2008] included the data from surface mixed layer where a Re_d - Ri_g relationship is clearly different from (19).

the proposed parameterizations are within the scatter of field data.

7. Discussion

[33] This study successfully parameterized momentum and buoyancy fluxes and the conversion rate of TPE to BPE using Fr_d^{-1} and Sh_d and constraints from (1) the limiting behaviors of l_E/l_d , Pr_b , α , and Ri_f ; (2) positiveness of Γ_d , α , and Ri_f ; and (3) the governing equations (7a) and (7b). To my knowledge, this is the first experiment-based mixing parameterizations that systematically include individual effects of shear and stratification. In particular, explicit parameterizations of shear effects on Γ and Γ_d (Figures 3a, 3b, and 5c–5f) are new results of this study. A by-product of this study is the parameterizations of various nondimensional turbulent quantities, which may be useful in the future (Table 3).

[34] For future assessments and improvements, potential issues of the proposed parameterizations are summarized in the following. First, Re_d effects may have been included during the fitting process because of strong correlation between Re_d and Fr_d^{-1} (Figure 1) and increasing trend of $(\Gamma_d - \alpha)/f_1$ with increasing Re_d (Figure 3f). The former is probably not so significant for f_2 and f_3 because their slopes with respect to Fr_d^{-1} are fixed from the constraints, but it would affect f_1 . Second, there is uncertainty in the behavior of l_E under strong stratification (i.e., $l_E \sim l_B$ or $l_E \sim l_O$). Third, Pr effects are considered to be significant [*Lienhard and van Atta*, 1990; *Smyth and Moum*, 2000; *Shih et al.*, 2005], but they are neglected in this study because the analyzed shear flow data do not show clear Pr dependence. Fourth, available data fill only limited part of the parameter space (Figures 2 and 3), and more data points at low Fr_d^{-1} and low Sh_d are required to refine fitting coefficients,

particularly Sh_d dependence. These points need to be investigated in the future, when more data become available.

[35] The proposed parameterizations can be directly compared to existing stability functions for two-equation turbulence closure schemes. These stability functions parameterize $c_\mu = \nu_t \varepsilon / E_K^2 = 4(P/\varepsilon)Sh_d^{-2}$ and $c_\mu' = \kappa_t \varepsilon / E_K^2 = 4(b/\varepsilon)Fr_d^2$ as functions of $\alpha_N = Fr_d^{-2}/4$ and $\alpha_M = Sh_d^2/4$ [*Burchard and Bolding*, 2001]. Stability functions by *Kantha and Clayson* [1994] and *Canuto et al.* [2001] (as presented by *Burchard and Bolding* [2001]) are chosen for comparisons. These stability functions clearly overestimate P/ε and b/ε under strong stratification (Figure 8). *Kantha and Clayson* [1994] and *Burchard and Deleersnijder* [2001] suggested an upper limit of $Fr_d^{-2} \approx 78$ and ≈ 25 for the stability functions by *Kantha and Clayson* [1994] and *Canuto et al.* [2001], respectively (the values are obtained using conversions among variables suggested by *Burchard and Bolding* [2001]); however, this does not prevent mixing with high efficiency under strong stratification. Also, both stability functions do not represent the increase of b/ε with increasing Sh_d at high Fr_d^{-1} (Figures 8c and 8d). Although homogeneous stratified shear flows represent only a special case in stratified shear flows in general, it would be preferable that general purpose mixing parameterizations reproduce the simplest case. The proposed parameterizations may be combined with two-equation closure schemes in principle, but parameterizations for unstable conditions are necessary for general-purpose models, and numerical stability has to be tested.

[36] The derivation of Ri_g -based parameterizations in this study provides some insight into their nature. It is well known that no set of coefficients for Ri_g -based parameterization is applicable to a wide range of conditions [e.g., *Lozovatsky et al.*, 2006, and references therein]. Equations (18a), (18b), and (19) suggest that one of the reasons is the variation of Re_{d0} , which is (using $Ri_{g0} = 0.1$ and $Sh_d = 10$) ≈ 600 for Lake Kinneret but $\approx 10^5$ for Hudson River estuary and the northern reach of San Francisco Bay (estimated from Figure 8 of *Peters* [1997] and Figure 18 of *Stacey et al.* [1999]). *Zaron and Moum* [2009] noticed that eddy viscosity and diffusivity vary nearly by an order of magnitude at the same Ri_g but in different depth ranges in the equatorial Pacific, and suggested that it is due to depth variation of mean flow conditions. This could also be due to the variation of turbulence intensity. This discouraged proposing Ri_g -based parameterizations of ν_t and κ_t for the equatorial Pacific and comparing them against previous models by *Pacanowski and Philander* [1981], *Peters et al.* [1988], *Large et al.* [1994], and *Large and Gent* [1999].

[37] The results of this study suggest that it is worth considering Sh_d as one of basic parameters to analyze field data, and investigating whether it causes systematic variations of, for example, Γ_d , l_E/l_d , α , and Γ in the field (Figures 3a, 3b, 4a, 4c, and 5c–5f). The proposed parameterizations are based on $l_d = q^3/\varepsilon$ due to advantages mentioned in Introduction. A disadvantage of this choice is that q is unavailable in common microstructure measurements (commonly available variables are N , l_T , l_O , ε , and χ). If one is interested only in the weakly stratified regime (low Fr_d^{-1}), a cut-off l_T/l_O of ≈ 1 may be used to exclude data in the strongly stratified regime, and a limiting (constant) value of l_E/l_d (Figure 4a) may be used to convert l_T to l_d . Note that the limiting value is

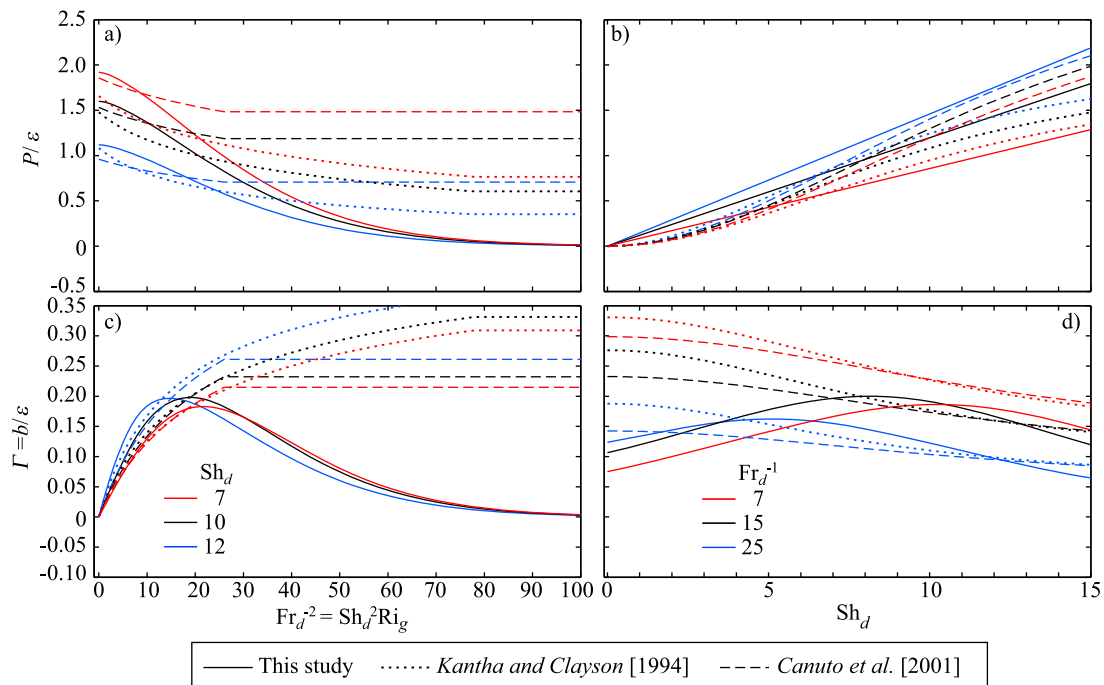


Figure 8. Comparison of proposed parameterizations and stability functions by *Kantha and Clayson* [1994] and *Canuto et al.* [2001]. For *Canuto et al.* [2001], parameter set A is used, and Fr_d^{-2} -capping suggested by *Burchard and Deleersnijder* [2001] is applied.

site specific (Table 4), possibly due to variation of Sh_d (Figure 4a), so it must be established with turbulent velocity measurements. If Sh_d takes a narrow range of values in the field, as in the self-similar stage of homogeneous stratified shear flows, parameterizations based on Sh_d and Fr_d^{-1} , such as those proposed in this study, would be more useful in the field because Fr_d^{-1} (hence q) and other turbulent quantities could be estimated from Γ_d (Figures 3a and 3b) or l_T/l_O .

[38] The analysis in this study considers turbulence generated only by mean shear, not by instability or stochastic internal waves that are important in oceans [e.g., *Gregg*, 1989; *Kunze et al.*, 1990; *Polzin et al.*, 1995; *Polzin*, 1996]. In homogeneous stratified shear flows, l_E/l_B and Γ_d increase toward ≈ 0.6 and ≈ 0.3 , respectively (and $l_E/l_O \approx 1.5$ but slowly increases with time). In turbulent collapse of Kelvin-Helmholtz instability, relevant to mixing due to stochastic internal waves, $l_T/l_O (\approx l_E/l_O)$ and Γ_d decrease rapidly toward ≈ 1 (but slowly decrease with time) and $0.2 \sim 0.4$ [*Smyth and Moum*, 2000; *Smyth et al.*, 2001]. This similarity between the two cases may be expected because l_E and l_O in the latter case become much smaller than the length scales of background shear and stratification [*Peltier and Caulfield*, 2003]. The difference of the driving mechanisms might be reflected in field data: oceanic data often show $l_E/l_O \approx 1$ and average Γ_d of $0.2 \sim 0.3$ [e.g., *Dillon*, 1982; *Moum*, 1996a, 1996b], whereas in lakes $l_E/l_O \ll 1$ is common [e.g., *Saggio and Imberger*, 2001; *Yeates*, 2008] and average Γ_d tends to be ≈ 0.15 [*Ravens et al.*, 2000; *Wüest and Lorke*, 2003]. Although the proposed parameterizations are comparable to oceanic data when normalized for turbulence intensity (Figure 6), this might be a special case because the data were

measured in the equatorial Pacific, where the equatorial undercurrent induces strong and persistent shear [*Peters et al.*, 1995]. Overall, the proposed parameterizations would be more relevant to coastal seas, estuaries, and lakes away from the boundaries, where mean shear is more important as a TKE source.

8. Conclusions

[39] This study proposed the parameterizations of non-dimensional momentum and buoyancy fluxes, P/ε and $b/\varepsilon = \Gamma$, and the conversion rate of TPE to BPE, Γ_d , as a function of $Sh_d = q^2 S/\varepsilon$ and $Fr_d^{-1} = q^2 N/\varepsilon$. The results show that Sh_d effects are important for P/ε , $b/\varepsilon = \Gamma$, and l_E/l_d , and cause relatively small but significant systematic variations on Γ_d , Pr_t , α , and Ri_f . The proposed parameterizations are within the scatter of limited field data, and detailed comparison is worthwhile in the future. This study also proposed a way to include turbulence intensity in Ri_g -based mixing parameterizations, and showed that existing stability functions for two-equation turbulence closure schemes are not consistent with laboratory and numerical experiments under strong stratification. The results of this study would serve toward better mixing parameterizations of different complexities.

Appendix A: Details of the Data Sets

[40] Primary data sources of this study are stratified shear flow data. From *Tavoularis and Corrsin* [1981], the data collected near the end of the wind tunnel ($x/h = 11$) are used because the temperature field was about to reach an asymptotic state there. $Ri_g = 0.002$ is mentioned in the paper,

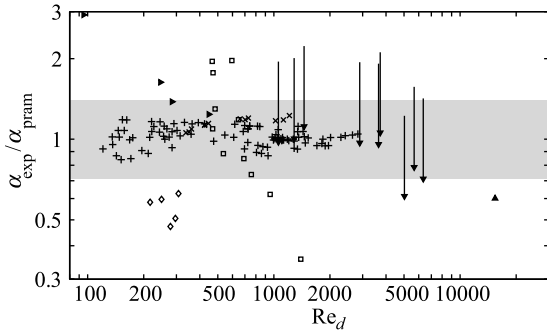


Figure A1. Ratio of measured α to parameterized α as a function of Re_d . The upper ends and lower ends (with symbols) of vertical lines show values before and after the bias correction for $\overline{\rho^2}$ from Rohr *et al.* [1988b] (inverted triangles). Data points from Stillinger [1981] also deviate from 1, but this is because the parameterized α does not capture the trend of the data very well (Figure 4c). Shading indicates fitting within a factor of 1.4. See Figure 1 for symbols.

but $Ri_g = 1.4 \times 10^{-4}$ is calculated from Table 4 in the paper; χ is not available in the paper and estimated from the equation for (half) the density variance

$$\bar{u} \frac{\partial}{\partial x} \left(\frac{1}{2} \overline{\rho^2} \right) = -\overline{\rho'w'} \frac{\partial \bar{p}}{\partial z} - \frac{1}{2} \chi. \quad (\text{A1})$$

Stillinger [1981] and Rohr *et al.* [1988b] collectively conducted water channel experiments at $Ri_g \approx 0, 0.07, 0.10, 0.22, 0.35, 0.7, 1.0, \text{ and } 1.3$. The buoyancy fluxes of Stillinger [1981] show significant oscillations after $x/M = 30$, and only data at $x/M = 20$ and 30 are used. The cases with the diffuser ($M = 0.01524$ m cases) used by Rohr *et al.* [1988b] are excluded because the flow did not reach a self-similar state. The $\overline{v^2}$ is not available in these data sets, and $\overline{v^2} = (27/73) (\overline{u^2} + \overline{w^2})$ is used to estimate q (see Appendix B). As suggested by Rohr *et al.* [1988b], χ is estimated from (A1) in an experiment in which $\overline{\rho^2}$ remains approximately constant at the later stage of the flow development (but after the following bias correction). The $\overline{\rho^2}$ from Rohr *et al.* [1988b] is consistently larger than other data sets by a factor of ≈ 2 . This can be seen by comparing the time series of α with DNS results by Shih *et al.* [2000, 2005] (not shown), or from fitting error of α (Figure A1). Furthermore, in a case χ is estimated, $\Gamma_d - \alpha$ is negative, but it should be positive from (13). Dividing $\overline{\rho^2}$ by 2 results in positive $\Gamma_d - \alpha$ and make the data consistent with other data sets. Therefore, $\overline{\rho^2}$ from Rohr *et al.* [1988b] is divided by a factor of 2 in this study. This affects l_E , but no correction is made to b . Based on DNS results, Itsweire *et al.* [1993] suggested that ε based on the longitudinal gradient of turbulent velocity is biased low by a factor of ≈ 2 in sheared flows. Although some bias is expected, no correction to ε is made to the data from Rohr *et al.* [1988b] because they report good collapse of velocity spectra at high wave number, and ‘correction’ of ε by a factor of 2 causes clear and significant bias compared to other data sets. In LES by Kaltenbach *et al.* [1994], molecular viscosity does not exist,

and Re_d is calculated based on the sub-grid scale viscosity, as done in their paper. They mentioned that high Ri_g runs ($Ri_g = 0.5, 1.0$) did not reach a self-similar state, so these runs are classified as decaying shear flows. The DNS database generated by Shih *et al.* [2000, 2005] includes model runs with $Ri_g = 0.04 \sim 1$. Only high initial Reynolds runs ($Re_\lambda \approx 89$, where Re_λ is the Reynolds number based on Taylor microscale) with $Pr = 0.72$ are used in this study. Grid switching at odd nondimensional time St causes some aliasing errors, which becomes more severe for higher Sh_d runs [Lee *et al.*, 1990]. For the self-similar shear flows, data points just before the grid switching are used to avoid aliasing errors. For the decaying shear flows, aliasing errors are smaller, and either latter half between the switching or all the data are used. The data from Webster [1964] and Piccirillo and van Atta [1997] are excluded due to low Reynolds numbers. High initial shear number cases [Lee *et al.*, 1990; de Souza *et al.*, 1995; Jacobitz *et al.*, 1997; Jacobitz and Sarkar, 1999] are also excluded because it is not clear whether these flows eventually reach a self-similar state or not.

[41] Unstratified shear flow data and unsheared stratified flow data are used to supplement the stratified shear flow data. A low initial Reynolds number run done by Rogers and Moin [1987] is included in order to show some Reynolds number dependence (Appendix B). Rose [1966] and Champagne *et al.* [1970], as well as cases L, M, N, O, and P of Tavoularis and Karnik [1989], are excluded as TKE did not show exponential growth in these experiments. For unsheared stratified experiments by Itsweire *et al.* [1986] and Lienhard and van Atta [1990], $\overline{v^2} = \overline{u^2}$ is assumed to estimate q , as done by Ivey and Imberger [1991]. Water channel data by Stillinger *et al.* [1983] are not used due to the lack of reported χ and availability of similar experiments by Itsweire *et al.* [1986]. Wind tunnel data by Yoon and Warhaft [1990] are excluded because the growth rates of TKE and TPE could not be calculated.

Appendix B: Reynolds Number Effects on B_{11} and B_{33} and the Estimation of $\overline{v^2}$

[42] Re_d effects are fortunately weak in many turbulence parameters, but they strongly affect $B_{11} = \overline{u^2}/q^2 - 1/3$ and $B_{33} = \overline{w^2}/q^2 - 1/3$ (Figure B1). A good collapse of B_{11} and B_{33} is obtained using $\varepsilon/(\nu S^2) = Re_d Sh_d^{-2}$, a nondimensional parameter used by Corrsin [1958], Itsweire *et al.* [1993], and Saddoughi and Veeravalli [1994]. In stratified cases, the interdependence of Sh_d , Fr_d^{-1} , and Ri_g makes it difficult to distinguish the effects of shear and stratification (e.g., $\varepsilon/(\nu N^2)$ gives worse but reasonable collapse); however, collapse of the data including unstratified shear flow cases by Rogers and Moin [1987] confirms that this is primarily due to shear being large compared to turbulence intensity. The increase and decrease of B_{11} and B_{33} with decreasing $\varepsilon/(\nu S^2)$ are approximately similar in magnitude, so $B_{22} = -B_{11} - B_{33}$ is more or less independent of $\varepsilon/(\nu S^2)$. Therefore, when $\overline{v^2}$ is unavailable, it is estimated as $(27/73) (\overline{u^2} + \overline{w^2})$, using $\overline{u^2}/q^2 = 0.51$, $\overline{v^2}/q^2 = 0.27$, and $\overline{w^2}/q^2 = 0.22$ [Tavoularis and Karnik, 1989].

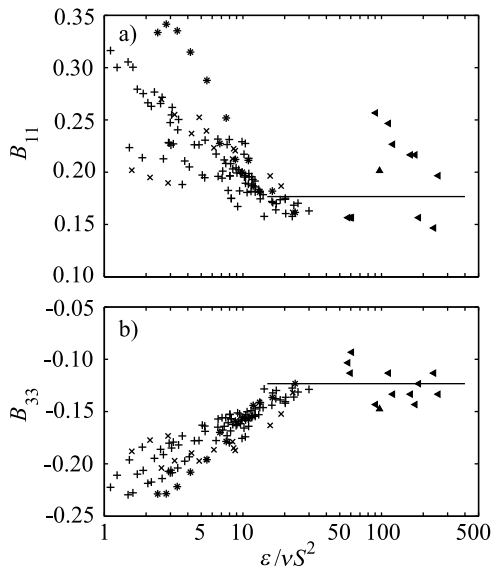


Figure B1. Dependence of (a) B_{11} and (b) B_{33} on $\varepsilon/(\nu N^2) = \text{Sh}_d^{-2} \text{Ri}^{-1} \text{Re}_d$. Solid lines indicate $B_{11} = 0.53 - 1/3$ and $B_{33} = 0.22 - 1/3$ suggested by *Tavoularis and Karnik [1989]* for unstratified shear flows. See Figure 1 for symbols.

[43] **Acknowledgments.** Special thanks to Lucinda H. Shih for kindly providing the DNS results of *Shih et al.* [2000, 2005], Parviz Moin for allowing me to use the DNS results of *Rogers and Moin* [1987], and Peter S. Yeates for helping me to plot Figure 7 with the data presented by *Yeates* [2008]. I thank Jeffrey R. Koseff, Gregory N. Ivey, and Keisuke Nakayama for their help to access some of the data sets, Gregory N. Ivey and Jochem Marotzke for their comments on an earlier version of the manuscript, and Steve Buchan and Michael Garvey for checking my English. Critical comments from anonymous reviewers were helpful to improve the quality of this paper. This paper was revised substantially while I am at Max-Planck-Institut für Meteorologie with the financial support of Klaus Hasselmann Postdoctoral Fellowship.

References

- Burchard, H., and K. Bolding (2001), Comparative analysis of four second-moment closure models for the ocean mixed layer, *J. Phys. Oceanogr.*, *31*, 1943–1968, doi:10.1175/1520-0485(2001)031<1943:CAOFMSM>2.0.CO;2.
- Burchard, H., and E. Deleersnijder (2001), Stability of algebraic non-equilibrium second-order closure models, *Ocean Modell.*, *3*, 33–50, doi:10.1016/S1463-5003(00)00016-0.
- Canuto, V. M., A. Howard, Y. Cheng, and M. S. Dubovikov (2001), Ocean turbulence Part I: One-point closure model—Momentum and heat vertical diffusivities, *J. Phys. Oceanogr.*, *31*, 1413–1426, doi:10.1175/1520-0485(2001)031<1413:OTPIOP>2.0.CO;2.
- Champagne, F. H., V. G. Harris, and S. Corrsin (1970), Experiments on nearly homogeneous turbulent shear flow, *J. Fluid Mech.*, *41*, 181–139, doi:10.1017/S0022112070000538.
- Corrsin, S. (1958), Local isotropy in turbulent shear flow, *Rep. RM 58B11*, 15 pp., Natl. Adv. Comm. for Aeronaut., Washington, D. C.
- de Souza, F. A., V. D. Nguyen, and S. Tavoularis (1995), The structure of highly sheared turbulence, *J. Fluid Mech.*, *303*, 155–167, doi:10.1017/S0022112095004216.
- Dillon, T. M. (1982), Vertical overturns: A comparison of Thorpe and Ozmidov length scales, *J. Geophys. Res.*, *87*, 9601–9613, doi:10.1029/JC087iC12p09601.
- Drennan, W. M., M. A. Donelan, E. A. Terray, and K. B. Katsaros (1996), Oceanic turbulence dissipation measurements in SWADE, *J. Phys. Oceanogr.*, *26*, 808–815, doi:10.1175/1520-0485(1996)026<0808:OTDMIS>2.0.CO;2.
- Ellison, T. H. (1957), Turbulent transport of heat and momentum from an infinite rough plane, *J. Fluid Mech.*, *2*, 456–466, doi:10.1017/S0022112057000269.
- Etemad-Shahidi, A., and J. Imberger (2001), Anatomy of turbulence in thermally stratified lakes, *Limnol. Oceanogr.*, *46*, 1158–1170, doi:10.4319/lo.2001.46.5.1158.
- Gargett, A. E., and J. N. Moum (1995), Mixing efficiencies in turbulent tidal fronts: Results from direct and indirect measurements of density flux, *J. Phys. Oceanogr.*, *25*, 2583–2608, doi:10.1175/1520-0485(1995)025<2583:MEITTF>2.0.CO;2.
- Gerz, T., U. Schumann, and S. E. Elghobashi (1989), Direct numerical simulation of stratified homogeneous turbulent shear flows, *J. Fluid Mech.*, *200*, 563–594, doi:10.1017/S0022112089000765.
- Gregg, M. C. (1989), Scaling turbulent dissipation in the thermocline, *J. Geophys. Res.*, *94*, 9686–9698, doi:10.1029/JC094iC07p09686.
- Harris, V. G., J. A. H. Graham, and S. Corrsin (1977), Further experiments in nearly homogeneous turbulent shear flow, *J. Fluid Mech.*, *81*, 657–687, doi:10.1017/S0022112077002286.
- Holt, S. E., J. R. Koseff, and J. H. Ferziger (1992), A numerical study of the evolution and structure of homogeneous stably stratified sheared turbulence, *J. Fluid Mech.*, *237*, 499–539, doi:10.1017/S0022112092003513.
- Itsweire, E. C., K. N. Helland, and C. W. van Atta (1986), The evolution of grid-generated turbulence in a stably stratified fluid, *J. Fluid Mech.*, *162*, 299–338, doi:10.1017/S0022112086002069.
- Itsweire, E. C., J. R. Koseff, D. A. Briggs, and J. H. Ferziger (1993), Turbulence in stratified shear flows: Implications for interpreting shear-induced mixing in the ocean, *J. Phys. Oceanogr.*, *23*, 1508–1522, doi:10.1175/1520-0485(1993)023<1508:TISSFI>2.0.CO;2.
- Ivey, G. N., and J. Imberger (1991), On the nature of turbulence in a stratified fluid. Part I: The energetics and mixing, *J. Phys. Oceanogr.*, *21*, 650–658, doi:10.1175/1520-0485(1991)021<0650:OTNOTI>2.0.CO;2.
- Jacobitz, F. G., and S. Sarkar (1999), On the shear number effect in stratified shear flow, *Theor. Comput. Fluid Dyn.*, *13*, 171–188, doi:10.1007/s001620050114.
- Jacobitz, F. G., S. Sarkar, and C. W. van Atta (1997), Direct numerical simulations of the turbulence evolution in a uniformly sheared and stably stratified flow, *J. Fluid Mech.*, *342*, 231–261, doi:10.1017/S0022112097005478.
- Kaltenbach, H.-J., T. Gerz, and U. Schumann (1994), Large-eddy simulation of homogeneous turbulence and diffusion in stably stratified shear flow, *J. Fluid Mech.*, *280*, 1–40, doi:10.1017/S0022112094002831.
- Kantha, L. H., and C. A. Clayson (1994), An improved mixed layer model for geophysical applications, *J. Geophys. Res.*, *99*, 25,235–25,266, doi:10.1029/94JC02257.
- Kunze, E., A. J. Williams III, and M. G. Briscoe (1990), Observation of shear and vertical stability from a neutrally buoyant float, *J. Geophys. Res.*, *95*, 18,127–18,142, doi:10.1029/JC095iC10p18127.
- Large, W. G., and P. R. Gent (1999), Validation of vertical mixing in an equatorial ocean model using large eddy simulations and observations, *J. Phys. Oceanogr.*, *29*, 449–464, doi:10.1175/1520-0485(1999)029<0449:VOVMIA>2.0.CO;2.
- Large, W. G., J. C. McWilliams, and S. C. Doney (1994), Oceanic vertical mixing: A review and a model with a nonlocal boundary layer parameterization, *Rev. Geophys.*, *32*, 363–403, doi:10.1029/94RG01872.
- Ledwell, J. R., E. T. Montgomery, K. L. Polzin, L. C. St. Laurent, R. W. Schmitt, and J. M. Toole (2000), Evidence for enhanced mixing over rough topography in the abyssal ocean, *Nature*, *403*, 179–182, doi:10.1038/35003164.
- Lee, M. J., J. Kim, and P. Moin (1990), Structure of turbulence at high shear rate, *J. Fluid Mech.*, *216*, 561–583, doi:10.1017/S0022112090000532.
- Lienhard V, J. H., and C. W. van Atta (1990), The decay of turbulence in thermally stratified flow, *J. Fluid Mech.*, *210*, 57–112, doi:10.1017/S0022112090001227.
- Lorke, A., F. Peeters, and A. Wüest (2005), Shear-induced convective mixing in bottom boundary layers on slopes, *Limnol. Oceanogr.*, *50*, 1612–1619, doi:10.4319/lo.2005.50.5.1612.
- Lozovatsky, I. D., E. Roget, H. J. S. Fernando, M. Figueroa, and S. Shapovalov (2006), Sheared turbulence in a weakly stratified upper ocean, *Deep Sea Res., Part 1*, *53*, 387–407, doi:10.1016/j.dsr.2005.10.002.
- Moum, J. N. (1996a), Efficiency of mixing in the main thermocline, *J. Geophys. Res.*, *101*, 12,057–12,069, doi:10.1029/96JC00508.
- Moum, J. N. (1996b), Energy-containing scales of turbulence in the ocean thermocline, *J. Geophys. Res.*, *101*, 14,095–14,109, doi:10.1029/96JC00507.
- Moum, J. N., D. R. Caldwell, J. D. Nash, and G. D. Gunderson (2002), Observations of boundary mixing over the continental slope, *J. Phys. Oceanogr.*, *32*, 2113–2130, doi:10.1175/1520-0485(2002)032<2113:OOBMOT>2.0.CO;2.
- Moum, J. N., A. Perlin, J. M. Klymak, M. D. Levine, T. Boyd, and P. M. Kosro (2004), Convectively driven mixing in the bottom boundary layer, *J. Phys. Oceanogr.*, *34*, 2189–2202, doi:10.1175/1520-0485(2004)034<2189:CDMITB>2.0.CO;2.

- Munk, W. H., and E. R. Anderson (1948), Notes on a theory of the thermocline, *J. Mar. Res.*, *3*, 276–295.
- Oakey, N. S. (1982), Determination of the rate of dissipation of turbulent energy from simultaneous temperature and velocity shear microstructure measurements, *J. Phys. Oceanogr.*, *12*, 256–271, doi:10.1175/1520-0485(1982)012<0256:DOTROD>2.0.CO;2.
- Oakey, N. S. (1985), Statistics of mixing parameters in the upper ocean during JASIN phase 2, *J. Phys. Oceanogr.*, *15*, 1662–1675, doi:10.1175/1520-0485(1985)015<1662:SOMPIT>2.0.CO;2.
- Osborn, T. R. (1980), Estimates of the local rate of vertical diffusion from dissipation measurements, *J. Phys. Oceanogr.*, *10*, 83–89, doi:10.1175/1520-0485(1980)010<0083:EOTLRO>2.0.CO;2.
- Pacanowski, R. C., and S. G. H. Philander (1981), Parameterization of vertical mixing in numerical models of tropical oceans, *J. Phys. Oceanogr.*, *11*, 1443–1451, doi:10.1175/1520-0485(1981)011<1443:POVMIN>2.0.CO;2.
- Peltier, W. R., and C. P. Caulfield (2003), Mixing efficiency in stratified shear flows, *Annu. Rev. Fluid Mech.*, *35*, 135–167, doi:10.1146/annurev.fluid.35.101101.161144.
- Peters, H. (1997), Observations of stratified turbulent mixing in an estuary: Neap-to-spring variations during high river flow, *Estuarine Coastal Shelf Sci.*, *45*, 69–88, doi:10.1006/ecss.1996.0180.
- Peters, H., M. C. Gregg, and J. M. Toole (1988), On the parameterization of equatorial turbulence, *J. Geophys. Res.*, *93*, 1199–1218, doi:10.1029/JC093iC02p011199.
- Peters, H., M. C. Gregg, and T. B. Sanford (1995), Detail and scaling of turbulent overturns in the Pacific Equatorial Undercurrent, *J. Geophys. Res.*, *100*, 18,349–18,368, doi:10.1029/95JC01360.
- Piccirillo, P., and C. W. van Atta (1997), The evolution of a uniformly sheared thermally stratified turbulent flow, *J. Fluid Mech.*, *334*, 61–86, doi:10.1017/S002211209600434X.
- Polzin, K. (1996), Statistics of the Richardson number: Mixing models and fine structure, *J. Phys. Oceanogr.*, *26*, 1409–1425, doi:10.1175/1520-0485(1996)026<1409:SOTRNM>2.0.CO;2.
- Polzin, K. L., J. M. Toole, and R. W. Schmitt (1995), Finescale parameterizations of turbulent dissipation, *J. Phys. Oceanogr.*, *25*, 306–328, doi:10.1175/1520-0485(1995)025<0306:FPOTD>2.0.CO;2.
- Polzin, K. L., J. M. Toole, J. R. Ledwell, and R. W. Schmitt (1997), Spatial variability of turbulent mixing in the abyssal ocean, *Science*, *276*, 93–96, doi:10.1126/science.276.5309.93.
- Ravens, T. M., O. Kocsis, A. Wüest, and N. Granin (2000), Small-scale turbulence and vertical mixing in Lake Bikal, *Limnol. Oceanogr.*, *45*, 159–173, doi:10.4319/lo.2000.45.1.0159.
- Rogallo, R. S. (1981), Numerical experiments in homogeneous turbulence, *Rep. TM 81315*, 94 pp., Natl. Aeronaut. and Space Admin., Washington, D. C.
- Rogers, M. M., and P. Moin (1987), The structure of the vorticity field in homogeneous turbulent flows, *J. Fluid Mech.*, *176*, 33–66, doi:10.1017/S0022112087000569.
- Rohr, J. J. (1985), An experimental study of evolving turbulence in uniform mean shear flows with and without stable stratification, PhD thesis, 266 pp., Univ. of Calif., San Diego.
- Rohr, J. J., E. C. Itsweire, and C. W. van Atta (1984), Mixing efficiency in stably stratified decaying turbulence, *Geophys. Astrophys. Fluid Dyn.*, *29*, 221–236, doi:10.1080/03091928408248190.
- Rohr, J. J., E. C. Itsweire, K. N. Helland, and C. W. van Atta (1988a), An investigation of the growth of turbulence in a uniform-mean-shear flow, *J. Fluid Mech.*, *187*, 1–33, doi:10.1017/S002211208800031X.
- Rohr, J. J., E. C. Itsweire, K. N. Helland, and C. W. van Atta (1988b), Growth and decay of turbulence in a stably stratified shear flow, *J. Fluid Mech.*, *195*, 77–111, doi:10.1017/S0022112088002332.
- Rose, W. G. (1966), Results of an attempt to generate a homogeneous turbulent shear flow, *J. Fluid Mech.*, *25*, 97–120, doi:10.1017/S0022112066000077.
- Ruddick, B., D. Walsh, and N. Oakey (1997), Variation in apparent mixing efficiency in the North Atlantic Central Water, *J. Phys. Oceanogr.*, *27*, 2589–2605, doi:10.1175/1520-0485(1997)027<2589:VIAMEI>2.0.CO;2.
- Saddoughi, S. G., and S. V. Veeravalli (1994), Local isotropy in turbulent boundary layers at high Reynolds number, *J. Fluid Mech.*, *268*, 333–372, doi:10.1017/S0022112094001370.
- Saggio, A., and J. Imberger (2001), Mixing and turbulent fluxes in the metalimnion of a stratified lake, *Limnol. Oceanogr.*, *46*, 392–409, doi:10.4319/lo.2001.46.2.0392.
- Schumann, U., and T. Gerz (1995), Turbulent mixing in stably stratified shear flows, *J. Appl. Meteorol.*, *34*, 33–48, doi:10.1175/1520-0450-34.1.33.
- Shih, L. H., J. R. Koseff, J. H. Ferziger, and C. R. Rehmann (2000), Scaling and parameterization of stratified homogeneous turbulent shear flow, *J. Fluid Mech.*, *412*, 1–20, doi:10.1017/S0022112000008405.
- Shih, L. H., J. R. Koseff, G. N. Ivey, and J. H. Ferziger (2005), Parameterization of turbulent fluxes and scales using homogeneous sheared stably stratified turbulence simulations, *J. Fluid Mech.*, *525*, 193–214, doi:10.1017/S0022112004002587.
- Smyth, W. D., and J. N. Moum (2000), Length scales of turbulence in stably stratified mixing layers, *Phys. Fluids*, *12*, 1327–1342, doi:10.1063/1.870385.
- Smyth, W. D., J. N. Moum, and D. R. Caldwell (2001), The efficiency of mixing in turbulent patches: Inferences from direct numerical simulations and microstructure observations, *J. Phys. Oceanogr.*, *31*, 1969–1992, doi:10.1175/1520-0485(2001)031<1969:TEOMIT>2.0.CO;2.
- Stacey, M. T., S. G. Monismith, and J. R. Burau (1999), Observations of turbulence in a partially mixed estuary, *J. Phys. Oceanogr.*, *29*, 1950–1970, doi:10.1175/1520-0485(1999)029<1950:OOTIAP>2.0.CO;2.
- Stillinger, D. C. (1981), An experimental study of the transition of grid turbulence to internal waves in a salt-stratified water channel, PhD thesis, 216 pp., Univ. of Calif., San Diego.
- Stillinger, D. C., K. N. Helland, and C. W. van Atta (1983), Experiments on the transition of homogeneous turbulence to internal waves in a stratified fluid, *J. Fluid Mech.*, *131*, 91–122, doi:10.1017/S0022112083001251.
- Tavoularis, S., and S. Corrsin (1981), Experiments in nearly homogeneous turbulent shear flow with a uniform mean temperature gradient. Part 1, *J. Fluid Mech.*, *104*, 311–347, doi:10.1017/S0022112081002930.
- Tavoularis, S., and U. Karnik (1989), Further experiments on the evolution of turbulent stresses and scales in uniformly sheared turbulence, *J. Fluid Mech.*, *204*, 457–478, doi:10.1017/S0022112089001837.
- Terray, E. A., M. A. Donelan, Y. C. Agrawal, W. M. Drennan, K. K. Kahma, A. J. Williams III, P. A. Hwang, and S. A. Kitaigorodskii (1996), Estimates of kinetic energy dissipation under breaking waves, *J. Phys. Oceanogr.*, *26*, 792–807, doi:10.1175/1520-0485(1996)026<0792:EOKEDU>2.0.CO;2.
- Thorpe, S. A. (1977), Turbulence and mixing in a Scottish loch, *Philos. Trans. R. Soc. London, Ser. A*, *286*, 125–181, doi:10.1098/rsta.1977.0112.
- Toole, J. M., K. L. Polzin, and R. W. Schmitt (1994), Estimates of diapycnal mixing in the abyssal ocean, *Science*, *264*, 1120–1123, doi:10.1126/science.264.5162.1120.
- Webster, C. A. G. (1964), An experimental study of turbulence in a density-stratified shear flow, *J. Fluid Mech.*, *19*, 221–245, doi:10.1017/S0022112064000672.
- Winters, K. B., P. N. Lombard, J. J. Riley, and E. A. D’Asaro (1995), Available potential energy and mixing in density-stratified fluids, *J. Fluid Mech.*, *289*, 115–128, doi:10.1017/S002211209500125X.
- Wüest, A., and A. Lorke (2003), Small-scale hydrodynamics in lakes, *Annu. Rev. Fluid Mech.*, *35*, 373–412.
- Yeates, P. S. (2008), Deep mixing in stratified lakes and reservoirs, PhD thesis, 127 pp., Univ. of West. Aust., Crawley, West. Aust., Australia.
- Yoon, K., and Z. Warhaft (1990), The evolution of grid-generated turbulence under conditions of stable thermal stratification, *J. Fluid Mech.*, *215*, 601–638, doi:10.1017/S0022112090002786.
- Zaron, E. D., and J. N. Moum (2009), A new look at Richardson number mixing schemes for equatorial ocean modeling, *J. Phys. Oceanogr.*, *39*, 2652–2664, doi:10.1175/2009JPO4133.1.
- Zilitinkevich, S. S., T. Elperin, N. Klecorin, I. Rogachevskii, I. Esau, T. Mauritsen, and M. W. Miles (2008), Turbulence energetics in stably stratified geophysical flows: Strong and weak mixing regimes, *Q. J. R. Meteorol. Soc.*, *134*, 793–799, doi:10.1002/qj.264.

K. Shimizu, Max-Planck-Institut für Meteorologie, Bundesstr. 53, Hamburg D-20146, Germany. (kenji.shimizu@zmaw.de)